Chapter 4

Total Scattering Experiments

Chapter Outline

4.1. GENERAL CONSIDERATIONS

4.1.1. Monochromatic Versus Polychromatic (Energy-Dispersive) Diffraction Methods

A powder diffraction experiment consists of measuring the scattered intensity as a function of momentum transfer, Q. As is clear from Eq. (2.6), the value of Q can be varied by changing either θ or $k(\lambda)$. The former corresponds to

Pergamon Materials Series, Vol. 16. http://dx.doi.org/10.1016/B978-0-08-097133-9.00004-6

the monochromatic beam angle-dispersive method, and the latter, the polychromatic (white) beam energy-dispersive method. In the former, Q is varied by varying the scattering angle at fixed energy, and in the latter, the diffraction pattern is determined by the spectroscopy of the diffracted beam at fixed angle.

For the case of X-ray diffraction, the method used by far the widest is the monochromatic angle-dispersive method because it is much more straightforward to collect and analyze the data. Only in situations where for other reasons it is necessary to have a fixed take-off angle does the energy-dispersive method tend to be preferred. The place where energy-dispersive measurements dominate is in the realm of time-of-flight (tof) neutron diffraction at spallation sources, which is the main method for obtaining neutron PDFs. As we discuss below, the time of arrival of the neutron depends on its speed, which also determines its wavelength, making energy-dispersive experiments straightforward: the energy of the arriving neutron need not be determined but only its time of arrival from which the energy is inferred. In these measurements, the Q-resolution is determined by the ratio of the size pulse length in time versus the neutron flight time, thus the ratio of the moderator to the length of the flight path, which can be 1:1000, achieving a Q-resolution of around 0.1%.

4.1.2. Single Crystal and Powder Diffraction Methods

The key to single-crystal diffraction measurements is to align the reciprocal lattice vector of the material, $\mathbf{K}$, to $\mathbf{Q}$ so that the Bragg condition, $\mathbf{K}=\mathbf{Q}$, is achieved (Eqs. 2.10 and 2.11). For this purpose, the sample orientation, as well as the diffractometer setting, has to be changed to achieve the maximum agreement of $\mathbf{K}$ and $\mathbf{Q}$. In the modern diffractometer, the orientation of the crystal is changed by a motorized goniometer that is run by a computer. Once the crystal orientation is recorded in the computer, the crystal and detector can be oriented to scatter from any desired Miller indices simply by specifying them.

Powder experiments are simpler since the sample is isotropic and there is no need to worry about the sample orientation. In this case, only the magnitude of Q is of importance. Varying Q is achieved by varying 2θ. It is important, however, that the powder is truly isotropic. Often because of gravity, stress, or surface, the powder is textured, that is, the crystalline grains are preferentially oriented. The diffraction data from a textured sample can be very misleading unless the texture is well characterized.

4.1.3. Accuracy of the Measurement

We now consider the general principles that govern the accuracy of the measurement. In discussing accuracy, it is important to separate accuracy in determining the Q-values and accuracy in measuring the intensity. The accuracy of the Q-values defining the positions of the Bragg peaks determines the

accuracy of the derived lattice parameters. It is relatively easy to obtain high accuracy in the Q-values by using a high-quality monochromator, good collimation, and good alignment. The intrinsic resolution of a monochromator is determined by its Darwin width, or mosaic spread if it is a mosaic crystal. The Darwin width can be calculated by using dynamical diffraction theory, but it can be rationalized by recognizing the fact that when the Bragg condition is met the X-ray can penetrate the crystal only by a certain amount even without absorption, since it is diffracted. This penetration depth, or the extinction length, λ_{ext}, defines the uncertainty in the momentum transfer by $\Delta q = 2\pi/\lambda_{ext}$. In practice, monochromator line widths are determined experimentally by measuring a rocking curve. This is accomplished by initially fixing θ and 2θ to fulfill the desired Bragg condition. The crystal is then "rocked" by varying θ at fixed 2θ.

The best way to obtain high collimation is to use a synchrotron radiation source that has a natural collimation due to the small source size and the large source-monochromator distance. The source size is defined by the size of the electron or positron bunch in the storage ring. Source-monochromator distances are generally more than 10 m and can be considerably longer than that, especially at third-generation synchrotron sources. The beam intensity remains high despite these long source-mono distances because of the relativistic squeezing of the radiation emitted by the electrons into a narrow cone around their direction of motion, that is, tangential to the ring. In high-resolution X-ray measurements using a synchrotron source, the resolution can approach the Darwin width of the monochromator, which is of the order of 10^{-5}. Thus, a lattice constant can be determined down to four decimal points. The resolution of neutron spectrometers is lower since neutron beams cannot be as highly collimated because of the lower source intensities. Presently, the best resolution achieved by neutron diffractometers is of the order of 10^{-3}. By curve fitting, however, the lattice constant can still be determined with the accuracy of 10^{-4}.

Of great importance in a PDF measurement is the accurate determination of the intensity of diffraction. This gives information about the position of atoms within the unit cell through Eq. (2.13). The intrinsic accuracy of the intensity measurement, $\Delta I/I$, is determined by the statistical accuracy of the particle count,

$$\frac{\Delta I}{I} = \frac{1}{\sqrt{N}}, \tag{4.1}$$

where N is the number of phonons or neutrons counted by the detector. However, the measured intensity is affected by other factors such as absorption, sample geometry, polarization, and the Debye–Waller factor, and it is not necessarily easy to correct for these effects with high accuracy. Thus, one has to use good judgment before accepting the atomic position determined down to many digits as is often published in the literature. Errors in measured intensities are discussed in more detail in Appendix 5.3.

4.2. THE NEUTRON SCATTERING EXPERIMENT

4.2.1. Sources

Neutrons for scientific studies are produced either at research reactors or at pulsed spallation neutron sources. The application of neutrons to research in materials goes back to the early days of neutron reactors in the 1940s (Schull, 1995). The other source of neutrons for research is the spallation source that was developed much more recently. The concept was tested at various laboratories in the United States, UK, and Japan in the 1970s (Carpenter, 1977). The first user facility, the Intense Pulsed Neutron Source (IPNS), started operations in 1982 at Argonne National Laboratory in the United States (Westfall, 2007). IPNS closed in 2008 but next-generation spallation neutron sources are running or under construction around the world and are among the most useful for PDF analysis because of the presence of many short-wavelength epithermal neutrons in the spectrum. However, reactor neutrons also yield very high-quality PDFs and have special characteristics that make them an interesting alternative, especially from diffractometers that look at a hot moderator such as D4 at the Institut Laue Langevin (ILL) in Grenoble, France, as we discuss below.

Pulsed neutrons can be produced either by an accelerator-based spallation method or by using a mechanical chopper at a reactor source. The latter are of no particular value for PDF work. In the spallation method, protons are accelerated to high energies ($\sim$1 GeV) and hit a target made of a heavy metal such as tungsten, mercury, or uranium. Through violent collision, protons shake down some neutrons from the nuclei of the target element by spallation, producing fast neutrons with the energy of several megaelectron volts. In a reactor, the fission process occurring in the nuclear fuel in the core of the reactor releases large fluxes of fast neutrons as a by-product. These exit the core where they are captured and moderated as described below before being made into beams. Research reactors differ from power reactors in that it is desirable to have a high flux density of neutrons and low power (which leads to less heating). The reactor core tends to be as small as possible and the reactor fuel as rich as possible in fissile material.

To be of use for materials diffraction, neutrons need to be slowed down to lower velocities and lower energies. In fact, the right neutron energies for this purpose correspond to thermal energies, of the order of k_BT, where k_B is Boltzmann's constant, with T in the vicinity of ambient temperature. The MeV hot neutrons thus need to be "thermalized" which is carried out in a moderator. The neutrons interact with some kind of matter which is maintained at a fixed temperature. The material is surrounded by neutron mirrors that reflect neutrons back into the material when they try and escape. Through inelastic collisions with the atoms in the material, the neutrons lose energy until they come into thermal equilibrium with the material. The neutrons then have a

Maxwell–Boltzmann energy distribution corresponding to the temperature of the material. A hole in the neutron reflectors allows the thermalized neutrons to escape the moderator and be formed into a beam for transporting to the experiment. The best moderator materials are those that have a high-incoherent inelastic scattering cross section, which are generally hydrogenous materials. Neutrons with temperatures around room temperature have wavelengths of around 1 Å; cold neutrons (from a moderator cooled to cryogenic temperatures) have wavelengths up to around 20 Å. For PDF work, we prefer relatively hot neutrons with wavelengths of a few tenths of an angstrom. You can get these from a hot moderator. For example, the spectrum from the hot moderator at ILL, which operates at 2000 °C, is peaked around 0.5 Å. The ILL hot moderator is made of graphite which is carefully insulated and is actually heated by the flux of gamma rays from the reactor core, another by-product of the fission process. There are not many hot sources at reactors in the world. As well as ILL (http://www.ill.eu), the LLB reactor at Saclay in France (http://www-llb.cea.fr/en/Web/main_e.php), and the FRM-II reactor in Munich, Germany (http://www.frm2.tum.de/en/index.html) have them, though the Munich reactor does not currently have a powder diffractometer on its hot source.

Spallation neutron moderators are similar to reactor moderators but have some important differences. For the spallation diffraction experiment, an important limitation in Q-resolution is the time-width of the incident pulse. The trick here is to get the high-energy neutrons from the spallation process into the moderator and then out of it as quickly as possible in a single bunch. As a result, it turns out that the neutrons are undermoderated, they do not come completely into equilibrium with the moderator before they leave, and the spectrum of neutrons has a significant tail of "epithermal" neutrons that are hotter than the thermalized ones. This epithermal tail provides a flux of short-wavelength neutrons that give the high-Q information in the total scattering experiment and is what makes spallation neutron sources often preferred for PDF measurements. In this way, short-wavelength neutrons can be obtained from a thermal moderator such as water, liquid hydrogen, or methane, and it is not necessary to have a hot moderator to get the short-wavelength neutrons at a spallation source. With such sources, Q_{max} values in excess of 100 $Å^{-1}$ are possible. Table 4.1 gives the existing (and proposed) sources and the instruments suitable for medium to high resolution, wide angle, total scattering, and PDF measurements at the time of writing. For convenience, Web site addresses are also included where more information can be obtained about these facilities and the procedures for obtaining beamtime.

4.2.2. Diffractometer

Neutron powder diffractometers can be split into two main categories: angle-dispersive diffractometers at reactor sources and tof diffractometers at

TABLE 4.1 Present and Future Neutron Sources and Instruments Suitable for PDF Measurements

Source	Location	URL	Instruments
European spallation source (ESS)	Lund, Sweden	http://ess-scandinavia.eu/	In preconstruction phase
Institut Laue Langevin	Grenoble, France	http://www.ill.eu/	D4
ISIS	Rutherford Appleton Laboratory, Chilton, Oxon, UK	www.isis.stfc.ac.uk/	NIMROD, POLARIS, GEM
J-PARC/MLF	Tokai, Ibaraki, Japan	http://j-parc.jp/MatLife/en/index.html	NOVA, iMATERIA SPICA, HI-SANS
MLNSC (Lujan Center)	Los Alamos National Lab, New Mexico, USA	http://lansce.lanl.gov/lujan/	NPDF, HIPD, PHAROS
Spallation neutron source (SNS)	Oak Ridge National Lab, Tennessee, USA	www.ornl.gov/sns/	NOMAD

spallation neutron sources.[1] PDFs can be obtained from either kind, though as discussed in Section 4.1.1, the tof method is more useful for high-resolution total scattering. Angle-dispersive neutron diffractometers resemble two-circle X-ray powder diffractometers that are described in more detail in Section 4.3; in fact, similar diffractometer hardware can often be seen at neutron and X-ray sources. However, because they are more useful for PDF measurements, we describe in greater detail tof diffractometers.

The diffractometer itself consists of a sample holder surrounded by fixed detectors. A collimated beam of neutrons emerges from the moderator close to the neutron source and travels down a beam pipe to the sample position. This is shown schematically in Fig. 4.1.

In total scattering measurements from crystals, a balance must be struck between Q-space resolution and intensity. Conventional wisdom was that PDF experiments are flux limited and the primary beam path should be as short as possible. What has become apparent more recently is that because of details of the strange Q-dependent asymmetric instrument resolution

1. A number of other more exotic possibilities deserve mention, such as tof diffractometers at reactor sources, Fourier diffractometers such as HRPD at JINR at Dubna in Russia, and so on, though they are not considered here.

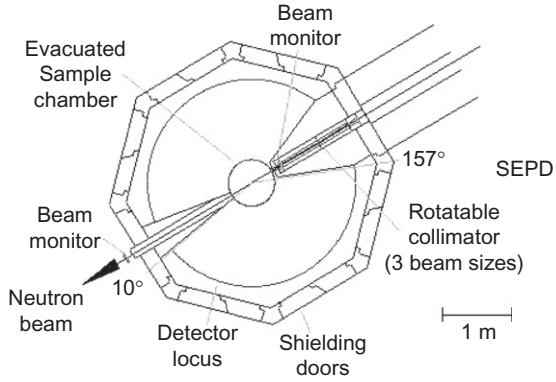

FIGURE 4.1 Schematic of a neutron time-of-flight powder diffractometer. The SEPD at IPNS, a first-generation tof diffractometer, is shown. This diffractometer has detectors arranged in banks in the scattering plane along the locus of the large circle.

function (a legacy of the non-Gaussian source spectrum), the Q-space resolution does affect the real-space resolution, and at least moderately, good Q-space resolution is desirable for high-quality total scattering and PDF work. Additionally, there is a trend emerging for studying samples using both conventional crystallographic methods (e.g., Rietveld refinement) and PDF, in which case Q-space resolution is clearly beneficial. The best compromise is an instrument on a relatively short flight path which still has a $\Delta d/d$ resolution of $\sim$0.2% or better. PDF instruments tend to be situated on primary flight paths in the range of 10–25 m. Diffractometers can be moved farther from the source without completely compromising the intensity with the use of neutron guides in the primary flight path. Unfortunately, these guides are very inefficient at propagating epithermal neutrons that give the important high-Q information in $S(Q)$ and do not result in performance gains for total scattering measurements.

The neutron beam is collimated, usually using boron containing rectangular-shaped inserts placed before the sample, into a beam of dimensions $\sim 2\ \text{cm} \times 4\ \text{cm}$. To optimize the scattering from the sample, it is therefore desirable to make the sample of similar dimensions. Samples generally are held in cylindrical containers made of natural abundance vanadium which is a metal that can be extruded and machined but which happens to scatter neutrons almost totally incoherently. It therefore contributes an almost smooth (tiny residual Bragg peaks remain) flat background that can be subtracted. The sample cans can be designed with seals allowing a heat-exchange gas (e.g., He for low-temperature measurements) to be incorporated which helps to keep the large sample in a state of thermal equilibrium with the sample environment not having to rely on inefficient heat conduction through the loosely packed powder. This results in rather small temperature gradients across the sample despite its large size. Other sample geometries are also used, for

example, wide flat samples are used on SANDALS and NIMROD at ISIS since most of the detectors are in the forward scattering direction on these instruments.

The secondary flight path is usually in the vicinity of 1–2 m. Low-angle detectors can be located further from the sample to compensate somewhat for their inferior resolution. The vicinity of the sample is usually evacuated to cut down air scattering and to facilitate the use of sample environments that require vacuum such as cryostats and furnaces.

The detectors sit at fixed angle and do not move. Instead, the intensity versus Q diffractogram appears as an intensity versus neutron energy spectrogram in each detector. The data consist of the histogram of neutrons that arrived at various time intervals after the generation of the incident pulse, as shown in Fig. 4.2. The tof, t, over the path, L, translates into the neutron velocity, $v = L/t$. This gives the momentum, $\hbar k = mv$, and the diffraction vector, Q, for elastic scattering by Eq. (2.6),

$$Q = \frac{2mL}{\hbar t} \sin\,\theta. \tag{4.2}$$

Thus, tof is inversely related to Q (Fig. 4.2).

In principle, the experiment could be carried out with a single energy-resolving detector at a fixed position. In practice, enormous gains in

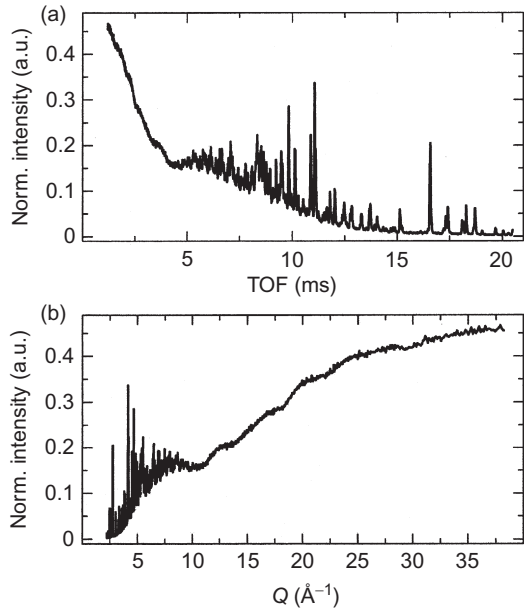

FIGURE 4.2 Data from SEPD showing intensity versus time-of-flight (a) from a crystalline sample of $Rb_3D(SeO_4)_2$. In (b), the same data are shown with the time-of-flight variable converted to Q using Eq. (4.2).

efficiency are possible by filling more solid angle with detectors. Early tof diffractometers had 10s or 100s of detectors which were grouped into "banks" centered at certain diffraction angles. The modern trend is to fill as much solid angle as possible with position-sensitive detectors (PSDs) which are pixilated to produce 3D dataset, two dimensions for $\boldsymbol{Q}$ and the third dimension for tof. This is immediately apparent by comparing the schematic of SEPD in Fig. 4.1 with those of NOMAD (Neuefeind *et al*., 2012) at SNS (Fig. 4.3) and NPDF (Fig. 4.4) at the Lujan Center at Los Alamos. NPDF (Proffen *et al*., 2002) was upgraded in 2002 from a conventional first-generation tof powder diffractometer to be optimized for total scattering and PDF measurements, and its layout before and after the upgrade are shown in Fig. 4.4 for comparison. GEM (Williams *et al*., 1998; Hannon, 2005) was designed and built from the ground up as a second-generation diffractometer and has 6500 detectors filling 3.5 steradians (sr) (out of $4\pi = 12.6$ sr). The detector coverage of NOMAD is even more aggressive and covers 3π sr. Beyond NOMAD, GEM, and NPDF, other examples are NIMROD (Bowron *et al*., 2010) and POLARIS (www.isis.stfc.ac.uk/instruments/polaris/) at ISIS and NOVA, iMATERIA (Ishigaki *et al*., 2009), and SPICA at J-PARC/MLF in Japan (http://j-parc.jp/researcher/MatLife/en/instrumentation/ns.html). NIMROD has many detectors in the forward scattering direction and is particularly suitable for studying complex liquids such as organics and is especially designed for handling hydrogenated materials, though it has low resolution. It also yields data over a wide range of Q including the low-angle region which may make it ideally suited to studying nanoparticles. POLARIS is undergoing an upgrade from the old instrument of that name as a medium-resolution high-throughput powder diffractometer and is expected to be an excellent instrument for PDF studies, including under *in situ* conditions. NOVA is a

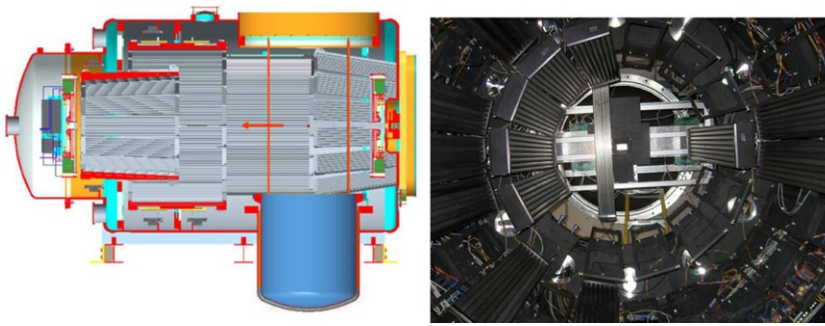

FIGURE 4.3 Detector configuration at a latest generation tof diffractometer, NOMAD at SNS, for comparison with an early diffractometer, SEPD, shown in Fig. 4.1. (Left) CAD drawings of the detector arrangements. (Right) Photograph of the inside of the detector tank showing the wide solid angle coverage of position-sensitive ^{3}He tubes.

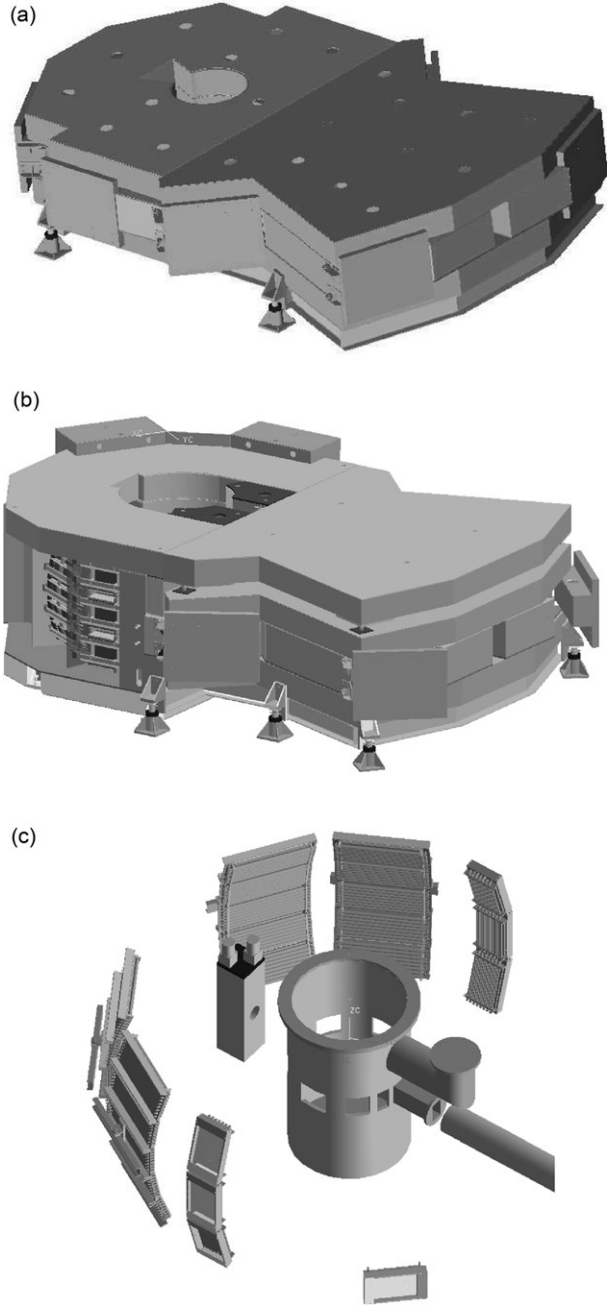

FIGURE 4.4 Schematic of the NPDF tof diffractometer at the Lujan Center at LANSCE before (a) and after (b and c) being upgraded from a conventional first-generation diffractometer to one optimized for total scattering studies. The exploded view in (c) shows the enormously enhanced detector coverage. The detectors are position-sensitive ^{3}He tubes. As a result of the upgrade, the number of detector pixels is increased from 62 to 6544 and detector area coverage is increasing from 4960 to 27,800 cm^2. The increase in detector coverage is concentrated in the important backscattering region.

high-intensity, low-resolution (0.35%) total scattering diffractometer. iMATERIA, whose full name is IBARAKI Materials Design Diffractometer, has a slightly higher resolution (0.16%) and a focus on high-throughput, small samples and supporting industrial users. SPICA is focused on measuring samples in special environments and has the highest Q-resolution of any of the J-PARC PDF diffractometers. Additionally, the High-Intensity Smaller Angle Neutron Scattering diffractometer (HI-SANS) at J-PARC, like NIMROD, combines small angle with wide-angle scattering, though it (unlike NIMROD) only has a maximum Q of 10 Å^{-1} but could be used for low real-space resolution PDFs. The Q_{max} of this instrument will change to 20 Å^{-1} in a forthcoming upgrade, greatly increasing its utility for PDF studies. Finally, as well as combining small-angle scattering (SAS) and PDF into a single instrument, very good PDFs have been obtained from an inelastic neutron scattering spectrometer, ARCS (Bozin *et al.*, 2009) at SNS, meaning that PDF and inelastic neutron scattering from powders may be readily combined in a single instrument. Inelastic PDF measurements, where the atomic correlations of correlated dynamics are measured directly, are discussed in detail in Chapter 7 although these are more challenging and time-consuming experiments than simply obtaining at PDF using the ARCS spectrometer as a diffractometer. PHAROS, the inelastic spectrometer at the Lujan Center of Los Alamos, is now primarily used for total scattering because its flux is too low to be competitive for inelastic studies. But it still retains its chopper and can be used to measure elastic as well as inelastic scattering intensities from the same sample. This capability is expected to be very useful in studying samples containing hydrogen. Many interesting samples contain hydrogen, and it is often impossible to replace all of them with deuterium. PHAROS will be able to sort out incoherent inelastic signals from hydrogen, allowing more accurate structural determination for samples containing hydrogen.

The diffractograms in each detector are shifted in energy, or tof, from each other due to the different diffraction angles (Eq. 2.2). In older diffractometers, detectors were grouped together in banks that had comparable resolution. The data from the detectors in a bank are combined by shifting the spectrum to account for the different position of the detector, a process known as "time-focusing." This was done electronically in early diffractometers to avoid the creation of large datasets from spectra of thousands of points from hundreds of detectors. With the increase in computer speed, and reduction in cost of data storage, this is no longer necessary, even with the thousands of detectors on modern instruments: spectra from individual detector elements are now typically stored. Thus, the size of the total data is huge, often of the order of gigabyte. The data corrections and reduction are then carried out using software allowing greater flexibility for choosing to include or exclude particular detector elements or to reprocess data *a posteriori*. A new mode for collecting data is "event mode," where the data are not histogrammed at all. In the histogramming process, neutron counts are assigned to detector pixel and tof

bins, and the counts in each bin summed over multiple pulses. In event mode, every detected neutron is individually recorded with its proton pulse, time of arrival, and detection location. This mode helps data streaming, which is continuous instead of intermittent and, in principle, allows the experimenter greater flexibility in postanalyzing data.

An important consideration with tof diffractometers for quantitative measurements is to have a stable, constant temperature moderator resulting in a time-stable incident spectrum. An example of the incident source spectrum from a spallation source is shown in Fig. 4.5. At lower power sources, the moderator material of choice has been solid or liquid methane that has good spectral characteristics for diffraction. Water moderators seem to have better stability making them attractive for PDF work, and the advantages of methane for conventional diffraction (more intensity at longer wavelengths, or lower Qs) are less apparent in total scattering measurements. The moderator for NOMAD at the SNS is supercritical liquid H_2. The peak in the thermal spectrum is moved to longer wavelength because of the low temperature of the moderator, but the high intensity of the source compensates and the stability of the moderator makes it work well for PDF studies.

Finally, data corrections are made for instrument-specific effects such as backgrounds and moderator instabilities (Chapter 5). These effects must be kept to a minimum for accurate PDFs to be determined. Fundamental additional requirements for the diffractometer therefore are low backgrounds, stable detectors and detector electronics, stable beam monitors, and a stable moderator. The low backgrounds are achieved primarily by excellent collimation and shielding, including a well-shielded primary beam dump or "get lost tube" (Fig. 4.1). Tight secondary collimation between the sample and the detectors is useful to lower backgrounds from special environments such as the heat shields from cryostats and furnaces, as well as lining the sample

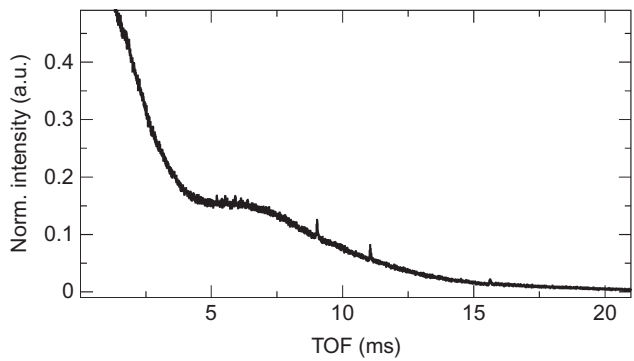

FIGURE 4.5 Example of a source spectrum from a spallation neutron source. The one shown is from SEPD at IPNS. It is measured using an incoherently scattering vanadium rod and some residual Bragg peaks are evident. Note the Maxwellian peaked around 7 ms crossing over into a quickly rising epithermal tail at short times (high energies).

can and secondary flight path with borated absorbing material. For the lowest backgrounds, oscillating radial collimators can be used. These solve the competing problems of wanting absorbing collimators in the secondary flight path (so only neutrons scattered at the sample position enter the detector) and wanting to fill solid angle with detectors. Radial collimators will tend to shadow the detectors, but by oscillating the collimators, no detector is shadowed all the time. Difficulties in reproducing these shadowing effects between samples can affect data corrections for PDF measurements and the radial collimation is often removed in practice.

Diffractometers at reactor sources work quite differently. As described in Section 4.2.1, the source spectrum is roughly a Maxwell–Boltzmann distribution peaked at the temperature of the moderator. The beam is collimated using a series of slits and a monochromatic beam is selected from this spectrum using a crystal monochromator. By way of example, D4 at ILL (Fischer *et al*., 2002) is currently the highest flux (5×10^7 N/cm^2/s) reactor neutron diffractometer on a hot source. The standard wavelength is 0.5 Å and detector banks cover to a maximum $2\theta = 140°$ that yields PDFs with Q_{max} 23.6 Å^{-1}. An advantage of the reactor source over the spallation source is that there is an increase in incident neutron flux with increasing Q, the opposite to a spallation source. The Q-resolution of reactor diffractometers is comparable to tof diffractometers. In the latter, the resolution depends on the length of the flight path and there is the normal trade-off between resolution and intensity. For reactor diffractometers, the Q-resolution is limited by the band-pass of the monochromator and the divergence of the incident beam. The Q-dependence of the resolution is governed by the standard Caglioti formulas (Caglioti *et al*., 1958; Hewat, 1975), improving at higher take-off angles. However, lower take-off angles are better for flux of short-wavelength neutrons and so instruments like D4 have a low take-off angle (22.4° compared to 135° for the high-resolution D2B) and a modest but reasonable resolution of $\Delta d/d \sim 2.5\%$. This is much better than the resolution of rapid acquisition PDF (RAPDF) X-ray measurements and quite acceptable for most PDF measurements.

Together with the absence of atomic form-factor effects relevant for electron and X-ray data, these characteristics actually make reactor neutrons quite interesting for moderate Q_{max} PDFs, and the use of D4 for PDF measurements on crystalline and nanocrystalline materials is currently growing and at the time of writing consumes roughly 25% of the available beamtime. Of particular interest at D4 is the very low background and tight secondary collimation (after the sample and before the detectors). D4 was designed in part for detecting small differences in isotope substitution measurements of glasses and liquids. To do this successfully, it is important to have extremely good count-rate stability and low backgrounds (including locating the diffractometer in a low-background part of the experiment hall!). These factors are also beneficial to PDF measurements on nanomaterials making D4 attractive when

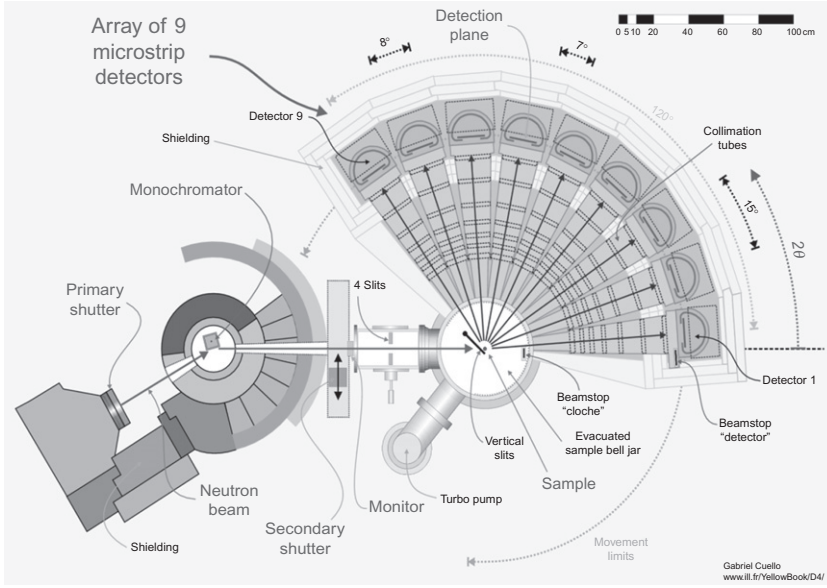

FIGURE 4.6 Schematic of the D4 diffractometer at ILL (Fischer *et al.*, 2002).

very high real-space resolution is not paramount (the D4 resolution function has an intrinsic r-space FWHM of 0.16 Å). The layout is shown in Fig. 4.6. It has nine ^{3}He (15 bar) 1D position-sensitive microstrip detectors. Each detector subtends an angle of 8° and each detector is separated by a 7° gap and data are collected by rotating all the detectors together in a block to cover the whole available range of Q-space. Another nice feature of reactor neutron diffractometers is the simple and well-characterized (Fischer *et al.*, 2012) instrument resolution function of, predominantly, Gaussian nature, and the greater simplicity and transparency of the data reduction procedures. These facts were recently used in a highlight of the synergy between PDFs being applied to crystalline and noncrystalline materials: PDFs of a crystalline calibrant were used with the fitting program PDFgui to calibrate the instrument resolution function yielding new insight into the physics of liquid eutectic samples (Chirawatkul *et al.*, 2011). Finally, there is excellent access to the sample position (somewhat easier than spallation source diffractometers, in general) making this diffractometer, and others like it, a candidate for measurements in custom sample environments. For example, a significant proportion of current experiments use high-volume Paris Edinburgh presses (Zeidler *et al.*, 2009; Drewitt *et al.*, 2010) or high temperatures in an aerodynamic levitation apparatus (Hennet *et al.*, 2006), and these environments are available for users.

4.2.3. Neutron Detection

Neutrons are weakly interacting neutral particles and are difficult to detect. The usual method is to incorporate a special isotope into a gas or a solid that captures neutrons and then decays quickly with the production of some strongly ionizing radiation such as high-energy protons. The problem then becomes to detect the ionizing radiation which is done using similar technologies to those used for detecting X-rays as discussed in Section 4.3.3.

The most common detectors use pressurized ^{3}He gas in a tube (Fig. 4.7). The relevant nuclear reaction in this case is $^3\mathrm{He} + \mathrm{n} \rightarrow \mathrm{p} + \tau + \gamma$ where n is the neutron, p is a proton, γ is a gamma ray, and τ is a triton, the nucleus of a tritium atom. The tube is constructed as a proportional counter with a wire down the middle that is maintained at a high voltage. The gas in the tube in the vicinity of the nuclear reaction is ionized by the high-energy proton and triton, and the ionized gas results in a charge pulse in the wire of the proportional counter. The charge pulse is swept out of the detector due to the applied voltage, amplified, converted to a digital pulse, and recorded in a computer. In tof diffractometers, the time of arrival of the neutron must also be determined accurately which is accomplished electronically. These ^{3}He tubes can also have a position sensitivity such that the position along the wire where the neutron arrived is also recorded. This is done by determining the relative time or arrival or pulse height of the positive and negative charge pulses at each end of the detector, the ratio giving the distance of arrival along the detector. These tubes are typically 1–2.5 cm in diameter and 0.5–1 m in length. The gas inside is typically a mixture of ^{3}He with small amounts of other gases (e.g., CF_4 or CH_4) for absorbing the proton and the triton more effectively and quenching the charge avalanche. To improve neutron detection efficiency, the gas is maintained overpressurized to a few atmospheres. To reduce background counts, it is desirable to lower the sensitivity of the detector to gamma rays by an appropriate choice of gas mixture. ^{3}He tubes are known for their

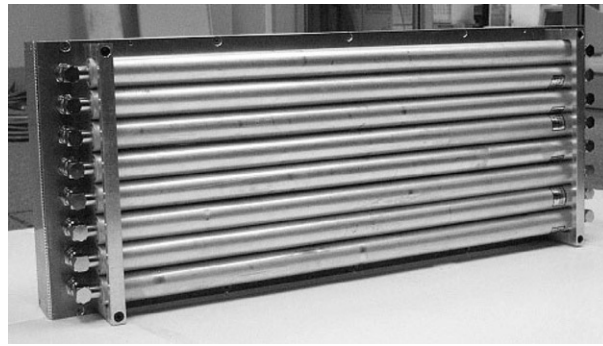

FIGURE 4.7 Photograph of a bank of ^{3}He tube position-sensitive detectors that are now installed on NPDF at the Lujan Center.

high detection efficiency, low sensitivity to gammas (gamma events generally have a lower pulse height (i.e., energy) than neutron events, allowing electronic discrimination of gammas in ^{3}He detectors), and adequate position sensitivity and count-rate capability. Another factor is the many years of experience with this kind of technology. A significant drawback moving forward is the worldwide shortage of ^{3}He. ^{3}He is produced by the decay of tritium and is a by-product of the nuclear weapons industry. The isotope was fairly abundant during the Cold War, but supplies are now dwindling with no plans for a large-scale ramp up in production that could satisfy world demand. With this in mind, it is especially interesting to find alternative isotopes for neutron detection. Other useful nuclei are ^{6}Li, ^{10}B, ^{155}Gd, and ^{157}Gd. The Li, B, and Gd isotopes tend to be used in scintillator detectors or as thin solid foils, though BF_3 is gaseous and can be used in a proportional counter similar to a ^{3}He tube. The ^{10}B isotope looks particularly promising as a longer term replacement for ^{3}He. A scintillator material is either doped with the absorbing nuclei or manufactured out of it (e.g., LiF or LiI). The nuclear reaction results in ionizing radiation that is absorbed by the scintillator that then gives off visible light. This light is shone onto an anode that emits electrons through the photoelectric effect. These are accelerated and amplified in a photomultiplier tube to produce a charge pulse that is converted to a neutron count. Position sensitivity is produced in these detectors by pixilating the detector and extracting light from each pixel using shielded optical fibers. An advantage of this technology is that the detector can be manufactured in any shape allowing solid angle to be filled very effectively with small amounts of dead area (see Fig. 4.8). Also, with improved commercial manufacturing processes used, the cost per steradian of these detectors is becoming rather low. Earlier problems with gamma sensitivity and low efficiency, especially for higher energy neutrons, are also now being successfully resolved. There is some probability that this technology will replace ^{3}He tubes in a number of applications.

4.2.4. Beam Monitor

Quantitative experiments such as total scattering measurements need to be normalized by the total neutron flux on the sample. This is accomplished by measuring the incident beam intensity using a beam monitor. Beam monitors are placed upstream of the sample (Fig. 4.1). In tof diffractometers, they usually consist of an incoherently scattering vanadium foil placed in the beam with one or more neutron detectors located off the axis of the beam. In order not to compromise the counting statistics of the measurements, it is desirable to have as many counts as possible in the monitor which is why multiple detectors around the vanadium foil are now considered desirable, as, for example, on GEM. If the incident spectrum from the moderator is very time stable, the spectrum in the beam monitor can be integrated over all energy

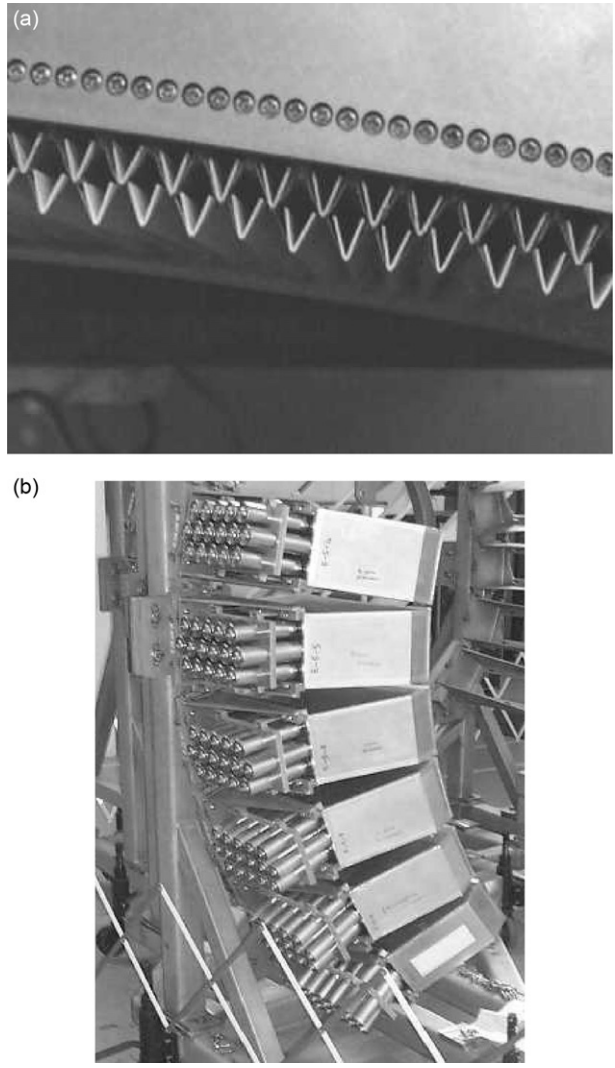

FIGURE 4.8 Photographs of scintillator detectors now installed on GEM at ISIS. (a) A close-up of V-shaped scintillator elements. (b) The elements built into space-filling modules with shielded photomultiplier tubes sticking out of the back of the modules. The light from the scintillator reaches the photomultiplier tubes via optical cables which cannot be seen inside the modules.

and just used to scale the intensities in the main detectors. However, it is sometimes preferred to normalize the detector spectrographs point by point by the monitor spectrograph to account for spectral instabilities. In this case, the spectrum from the beam monitor is often smoothed (it contains no sharp features anyway), so counting statistics becomes less of an issue, although

there is the possibility that this smoothing introduces systematic errors. These days, moderator stability and adequate beam monitoring are probably the accuracy limiting factors in most tof neutron PDF measurements, and they are receiving renewed attention in current- and next-generation diffractometers.

One of the key parameters required in the data analysis (Chapter 5) is the total scattering cross section of the sample. This depends on energy but, to a good approximation, is inversely related to the neutron energy. It is often, therefore, calculated theoretically knowing the neutron scattering cross sections of the constituents (measured traditionally at 1.3 Å neutron wavelength) and the sample density and size (therefore the number of scatterers), and using the approximate energy dependence mentioned above. A more precise determination of the total attenuation cross section can be made if a second beam monitor is placed after the sample (Fig. 4.1). The ratio of the two monitors then gives a measure of the sample attenuation cross section as a function of energy. This is not done on most utilitarian tof powder diffractometers due to engineering difficulties and lack of enthusiasm.

At reactors, beam monitors are typically either ^{3}He detectors in the incident beam path, when higher detection efficiency is desired, or a wire or foil coated with ^{235}U enriched uranium, when a lower detection efficiency is preferred (detection efficiency should always be low—$\sim 10^{-5}$—or the direct beam will not get through!). This is the setup at D4 at ILL. This kind of beam monitor is exceptionally stable, though next-generation diffractometers are unlikely to be built this way because of the more difficult regulatory environment surrounding the use of enriched uranium. A third type that is being developed but is not fully tested yet is a 1–2 bar nitrogen proportional counter setup.

4.2.5. Measurement Geometry

Because of the fixed detector geometry, wide solid angle coverage, and rectangular beam shape, the normal geometry of the measurement both at spallation and reactor sources is to have cylindrical samples.[2] This is particularly appropriate in previous generation diffractometers where all of the detectors were arranged in the (horizontal) scattering plane at the same height as the sample. This geometry is the most natural when multiple detectors at different angles are used. Current- and next-generation diffractometers have detectors that sit above and below the scattering plane. In this case, a square or circular beam and spherical samples would be the most natural geometry, though to date, the cylindrical sample shape has been retained for practical reasons: ease of making and filling sample cans. If the strongly off-axis detectors have

2. As described above, the old SANDALS and the new NIMROD diffractometers actually use a flat-plate sample geometry.

spectra that cannot be corrected, the beam dimensions can be changed to be more square, or these detectors can be left out of the analysis. So far, this seems not to be a significant problem.

4.3. THE X-RAY SCATTERING EXPERIMENT

4.3.1. Sources

The most commonly used X-ray generator is a system having a sealed tube with a copper (Cu) target (see Klug and Alexander, 1974; for detailed descriptions of conventional sources and measurement geometries). The characteristic K_α X-rays generated by such a tube have the wavelength of 1.544 Å and a wave vector magnitude of $k_0 = 4.069$ Å^{-1}. This, however, limits the range of Q to be below 8 Å^{-1} since $\sin\theta < 1$ so $Q_{max} < 2k_0$ (Eq. 2.2). Consequently, only a few diffraction peaks can be detected by using such a system. Let us suppose that N diffraction peaks were recorded by the powder diffractometer. This translates to $2N-1$ pieces of information, as the position and the intensity of each peak provide $2N$ numbers as a dataset, while the normalization of the intensity usually is not in the absolute scale, thus unknown. If the structure is fully crystalline and the number of parameters is less than $2N-1$, this set of numbers can fully determine the structure. However, aperiodic deviations from the periodicity cannot be described by such a small set of parameters and require a larger range of Q-space over which the data must be measured.

For the highest resolution and accuracy measurements, the use of an X-ray synchrotron source is preferred as we describe below. However, perfectly acceptable low- and medium-resolution PDFs can be obtained in the laboratory. The range of Q-space accessible with the readily available sealed tubes is limited as shown in Table 4.2. Molybdenum tubes give relatively good flux

TABLE 4.2 X-Ray Energies, Wavelengths, and Approximate Q_{max} Values for Common Laboratory X-Ray Sources

Source	E_0 (keV)	λ (Å)	Q_{max} (Å^{-1})
Cu	8.05	1.538	8.0
Mo	17.48	0.708	17.5
Ag	22.16	0.559	22.0
W	59.32	0.209	59.0

Energies shown are the $k_{\alpha 1}$ emission energies. The Q_{max} values are calculated assuming a maximum accessible scattering angle of 160°. Note the convenient property that the Q_{max} value in Å^{-1} is almost the same as the X-ray energy in keV. A useful resource for finding X-ray properties of elements is the *X-ray Data Book* published by Lawrence Berkeley National Laboratory and available online at http://xdb.lbl.gov/.

and will yield $S(Q)$ up to Q_{max} of around 14–15 $Å^{-1}$. This kind of source is often used for laboratory liquid and amorphous measurements and provides a good workhorse for low-resolution basic sample characterization type measurements. Silver tubes give Q_{max} of around 20–21 $Å^{-1}$ which can be satisfactory (though not optimal) for PDF measurements even in crystalline materials at room temperature. However, the big trade-off is a significant reduction in intensity, even from the low intensities of Mo tubes. This results in very long measurement times. Traditionally, measurement times of a number of days' duration are not unusual with silver sources and adequate statistics at higher Q-values may mean measurements running into the range of weeks. This is now being addressed by the X-ray instrument manufacturers as they start to market laboratory X-ray sources optimized for PDF measurements. With the use of modern microfocus X-ray tubes; multilayer optics, which are only now becoming available for Mo and silver sources; and parallel counting 1D and 2D detectors, this wisdom is set to become rapidly obsolete allowing rather good PDFs to be obtained from laboratory sources in reasonable time in the future.

The power, and therefore the flux, from a laboratory source can be increased by the use of a rotating anode source. This gives an increase in flux of approximately five times over an equivalent sealed tube source. Rotating anode instruments are beginning to go out of favor because of the relatively high maintenance, combined with the fact that similar gains in intensity are possible from multilayer optics and other advances in modern instrumentation such as microfocus sources. These days, desktop X-ray sources that use just a few hundred watts of power are producing X-ray fluxes on the sample comparable to the complex and difficult-to-use rotating anodes of yesteryears.

The preferred source of X-rays for PDF work is synchrotron radiation. Synchrotron X-rays are found at large-scale user facilities dotted around the globe and scientists gain access to these facilities by writing scientific user proposals for their experiments. The beamtime is generally given out for free after a peer-review process of the proposed experiments. When getting started using synchrotron X-rays for the first time, it is advisable to contact one of the instrument scientists at a beamline where PDF studies are carried out. They can provide help and advice for the whole process from proposal writing to carrying out the experiment, and even, often, on the data analysis and interpretation afterward.

The synchrotron source produces an intense, white X-ray beam that can be used either as is as a white beam or, more commonly, monochromatic beam using a single-crystal monochromator. There are now a large number of synchrotron X-radiation sources operating in the world. At the time of writing, the extensive list of X-ray storage rings on the lightsources.org Web site listed 69 sources either operating or under construction in countries across the globe. A number of these are soft X-ray or ultraviolet beamlines that are unsuitable for PDF measurements. The sources with an electron energy of

2.5 GeV or greater are required for PDF work on crystals. The newer "third-generation" sources such as the European Synchrotron Radiation Facility (ESRF) (Grenoble, France, http://www.esrf.eu/), the Advanced Photon Source (APS) (Argonne National Laboratory, Illinois, USA, http://www.aps.anl.gov/), SPRING-8 (Harima, Japan, http://www.spring8.or.jp/), NSLS-II (Brookhaven National Laboratory, New York, USA, http://www.bnl.gov/ps/), Diamond Light Source (Rutherford Appleton Laboratory, Oxfordshire, UK, http://www.diamond.ac.uk/), Soleil (Saclay, France, http://www.synchrotron-soleil.fr/), PETRA-III (http://petra3.desy.de/), and so on feature high luminosity in addition to high intensity at high X-ray energies. Many scattering experiments which have been impossible or impractical so far are now feasible. With the growth of the PDF technique, there are now a number of beamlines that are optimized for PDF measurements either operating or under construction at these sources, including at the time of writing, 11IDB and C at APS, XPD at NSLS-II, ID11 and ID15 at ESRF, and XPDF at Diamond, though these beamline designations tend to change with time due to facility upgrades and new construction. The current status can be found at facility Web sites.

Synchrotrons produce high fluxes of X-rays with tunable wavelengths. The flux of X-rays at different energies depends on the characteristic energy of operation of the synchrotron ring itself and on details of the beamline source and optics, such as whether it has an insertion device such as a wiggler or undulator. A number of books and resources are available describing the characteristics of X-ray synchrotron sources. One of the best resource for background information on both synchrotron radiation and its use as a scattering probe is the book by Als-Nielsen and McMorrow (2011). Another recent introductory text is Willmott (2011). The lightsources.org Web site is another resource as it maintains a page of introductory and educational material.

Synchrotrons can be used to make traditional PDF measurements with a point detector rotated through wide angular ranges. In this case, the main difference from laboratory sources is that the incident beam is very parallel and not divergent (and also, typically, higher in flux). However, the availability of high fluxes of high-energy X-rays at modern synchrotron sources have revolutionized the PDF method is through the use of large area 2D detectors and the RAPDF method (described in Section 4.3.2.1).

4.3.2. Diffractometer

4.3.2.1. RAPDF Method

Since the development of the RAPDF method in 2003 (Chupas *et al.*, 2003), there has been considerable growth in the application of PDF methods to problems in materials science, chemistry, and physics. The reason is that PDF transitioned from a difficult-to-carry-out and time-consuming experimental proposition, requiring considerable expertise in scattering, and not to mention

the theory and practice of data analysis and modeling, to something much more straightforward. At a stroke, RAPDF made the experiments both much easier to carry out and much quicker. This opened up the method to a much larger audience of people who needed local structural information to solve their scientific problems, but who did not want to dedicate their lives to learning arcane scattering methods.

The RAPDF measurement is extremely straightforward. There are basically no moving parts. A high-energy monochromatic incident beam is incident on the sample. A large area 2D detector is placed orthogonal to the beam and normally placed as close as possible behind the sample. This is shown in Fig. 4.9. A representative diffraction pattern from a RAPDF experiment is shown in Fig. 4.10. In the figure, the setup shows a four-circle diffractometer, but this is not required for this experiment. The experiment would work with the sample mounted in a stationary fashion on a post.

The geometry of the sample is sometimes pill-shaped and sometimes a capillary. The pill-shaped sample, with the beam and the diffraction being transmitted in the forward direction through the sample which is highly transparent at the high X-ray energies used, is actually a better geometry for the

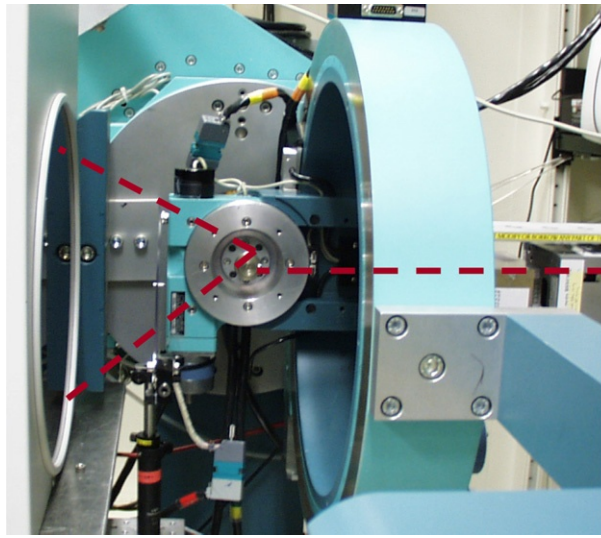

FIGURE 4.9 Photograph of the RAPDF setup. An intense high-energy X-ray beam (typically 60–100 keV) comes from the right. The sample is placed at the center of the circle in the center of the picture. The large area 2D detector, in this case, a MAR345 image plate detector, is placed orthogonal to the beam and behind the sample. The closer the detector is to the sample, the wider the Q-range that is detected for a given incident X-ray energy. This figure shows the sample mounted on a four-circle diffractometer which was present in this particular X-ray hutch (6ID-D at APS). However, this is not necessary. The sample could be simply mounted on a post or a spinner if it is desired to obtain better powder statistics.

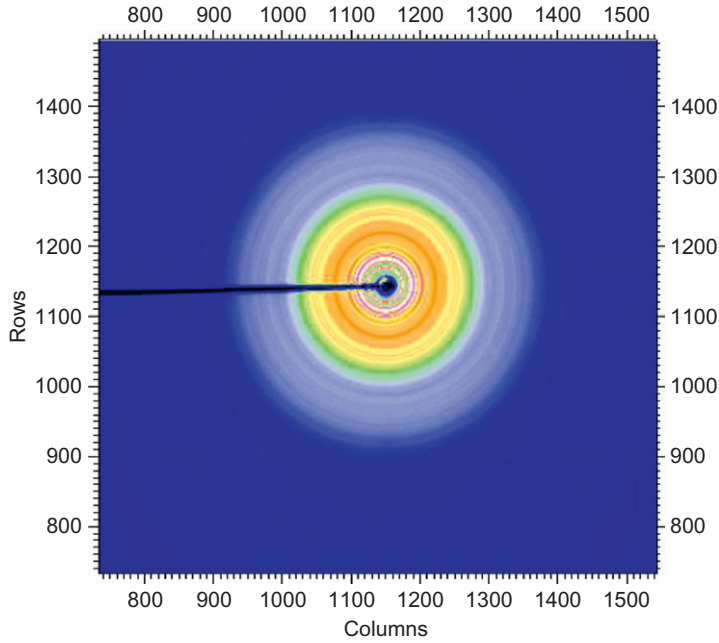

FIGURE 4.10 A representative 2D diffraction pattern from a RAPDF experiment. The circularly symmetric rings are the Scherrer rings of the powder pattern from the sample. The black object in the image is the beam stop that prevents the intense incident beam hitting (and damaging) the detector.

setup. However, it is rarely used for reasons of convenience. There are a number of reasons why samples mounted in a capillary are easier to handle; they also yield data of indistinguishable quality and so are now generally preferred. The preferred diameter of the sample capillary or pill depends on the scattering power of the sample. Normally, 1-mm internal diameter capillary tubes are loosely filled with powder and mounted on a goniometer head, or other support. For weakly scattering samples, such as organics, it may be preferable to use 2 mm ID tubes so that more signal is obtained from the sample. The trade-off is that the resolution of the measurement will be lower due to geometric effects and the finite size of the sample, so smaller ID capillaries are preferred when scattered intensity is not an issue.

The capillary is mounted with its long axis perpendicular to the beam but may be mounted vertically or horizontally (or at any other orientation perpendicular to the beam). The horizontal mounting seems to be easier when the sample is being cooled using a flowing nitrogen cryocooler, though this is by no means the only mounting geometry as the sample itself is an isotropic powder of micro- or nanograins and so could be presented to the beam at any angle in principle. It is often desirable to spin the capillary about its long

axis to improve powder statistics in the diffraction pattern. This spinning has a large effect on the powder statistics and is highly desirable if the data appear a bit spotty. This may be done with a rather low-tech solution of a simple electric motor rotating a goniometer on which the sample is mounted. The speed of rotation should preferably be much faster than the exposure time so that many revolutions fit into the exposure. The sample rotation can also be carried out by mounting the sample on a goniometer circle driven by stepping motors. In a less ideal case, but still better than nothing, the sample may be stationary during exposure but subsequent repeat exposures taken at different rotation angles. This kind of solution may be necessary if the sample is in a special environment with a large moment of inertia that cannot be rotated quickly, such as a displex cold stage, for example.

For ease of handling and relatively weak scattering power, capillaries made of polyimide (sometimes called kapton tubing) are often used. These come in the form of straws that can be cut to length with scissors. The end is sealed with either clay or a glue such as epoxy. The tube is then filled with the sample and capped off, again with clay or epoxy. Such samples are less liable to breaking during transportation, though when they contain liquids, the liquids have been known to escape during shipping, in which case, a glass capillary may be preferable. Polyimide tubing may also transmit some oxygen through it too, and so it may be preferable to seal very air-sensitive samples in glass.

A large area 2D detector is placed perpendicular to the beam and around 200 mm behind the sample. The distance is chosen to yield the desired Q_{max} for the given wavelength, though often the actual distance is decided by physical constraints in the setup preventing the detector to be moved closer to the sample. The direct beam is often aligned to the center of the detector. This nicely matches the geometry of the detector to the geometry of the measurement and ensures that the whole Scherrer ring is collected in the critical, and signal-limited, high-Q region. This is the preferred geometry unless one of the factors below dictates otherwise. If the energy of the incident beam is not high enough to access the desired Q_{max} with this setup, Q_{max} can be increased by offsetting the detector to the side so the direct beam hits the edge of the detector or just misses the side of the detector. In this way, a cake slice of the full diffraction pattern is obtained, either half or a quarter of the pattern depending on whether the incident beam is centered on the edge or the corner of the detector. In modern RAPDF setups, it is desirable to allow the detector to be moved parallel to the beam either closer or further from the sample so that the competing requirements of Q_{max} (closer) and Q-space resolution (farther) can be optimized. One can have one's cake and eat it by collecting data with the detector first close and then far for the same sample conditions. An emerging trend is to collect SAS data at the same time as PDF data. The SAS data may be used to determine nanoparticle size, as opposed to nanocrystalline domain size obtained by the PDF measurement (Farrow and Billinge,

2009) as discussed in Chapter 3. By the standards of real SAS measurements, which generally aim to study much larger particles, as large as micron scale, the SAS from small nanoparticles of interest in a PDF measurement is relatively easy to obtain and would probably be considered wide-angle data to a SAS person. To differentiate it from real specialized SAS measurements, which implies rather sophisticated technologies to obtain quantitative intensities at very small angles, we sometimes refer to these measurements as "medium-angle scattering," so as well as SAXS and WAXS, we have MAXS. Such data can be readily obtained using the same setup as the RAPDF measurement, but moving the detector back much further, that is, a number of meters, behind the sample. Since it may be desired to obtain PDF and MAXS data from the sample under identical conditions, for example, in an *in situ* measurement, it may be possible to mount two detectors, both perpendicular to the beam but one near and one far from the sample. On the wish list for the future would be a large area 2D detector with a small hole in the middle. This would make it very straightforward to daisy-chain multiple detectors at different distances and obtain simultaneously PDF data, higher resolution wide-angle diffraction data and MAXS data. It would also do away with the need for (and background scattering from) a beam stop. No such detector currently exists.

A small beam stop made of a heavy metal is placed just in front of the detector to accept and absorb (as much as possible) the direct beam and prevent it from damaging the detector. This often has a cup shape to shield the detector from scattering from the beam stop itself. It should be as small as possible while still accepting the full beam. It is generally placed as close as possible to the detector so that as little of the low-Q region of the diffraction pattern as possible is cut off. This has the slight disadvantage that there is a significant path through air for the direct beam to travel after the sample, which contributes significant air scattering as a background. This could be reduced by filling this region with a weaker scattering material such as He. However, practical difficulties, along with the fact that the air scattering background is undesirable but rarely problematic, mean that this is hardly ever done.

Different detector technologies may be used, as discussed below. Preferable performance characteristics are for the detector to have a large dynamic range where it is linear, and preferably a low background and dark current. Image plate detectors provide these characteristics but have slow readouts which often become the limiting criterion for the time resolution of the measurement. Data may be collected in a second or less but the detector takes 100 times longer to read out, so the experimental overhead is absolutely dominated by detector readout. A good compromise between fast readout and acceptable dynamic range and noise characteristics are provided by the amorphous silicon detectors that were originally developed for medical imaging, marketed, for example, by PerkinElmer and General Electric. Other large area

2D detectors such as the ESRF Frelon and the Swiss Light Source Pilatus detectors also work well. In the future, it is hoped that affordable, large area, high count-rate energy-resolving detectors with high dynamic range will become available. This would reduce backgrounds in the detector from inelastic scattering processes such as Compton and fluorescence. However, in the mean time, and slightly surprisingly perhaps, the nonenergy-resolving integrating detectors currently in use are proving enormously powerful.

The RAPDF experiment has one final huge advantage. For a number of reasons, it is almost ideally suited to *in situ* measurements. First, the incident beam energy is very high, and so the X-rays are very penetrating. They can get into and out of a high-pressure diamond anvil cell or a reaction vessel or flow cell. There are really no moving parts, so a static setup is possible for the *in situ* device, easing the design criteria for the device and making alignment much more straightforward. The diffraction all takes place in the forward scattering direction, so a relatively small X-ray transparent window needs to be built into the *in situ* device. Finally, the intense synchrotron beams can be made small, provided that powder averaging issues do not become limiting. Consequently, there is huge growth and great interest in the use of PDF methods for *in situ* and *in operando* (working devices in the beam) experiments.

4.3.2.2. Conventional Point Detection Strategies

A two-circle diffractometer is all that is required for these measurements, though typically beamlines are equipped with four- or six-circle diffractometers. The two circles are denoted θ and 2θ. This is shown schematically in Fig. 4.11. They are coaxial, but the θ circle rotates the sample and the 2θ circle the detector. As the naming scheme suggests, the circles are linked in such a way that the detector moves at twice the rate of the sample. This is discussed in more detail in Section 4.3.5. A similar, though less common, arrangement is the so-called θ–θ geometry. This is useful for the measurement of samples that must remain horizontal and cannot be tilted, in particular, liquids. In this

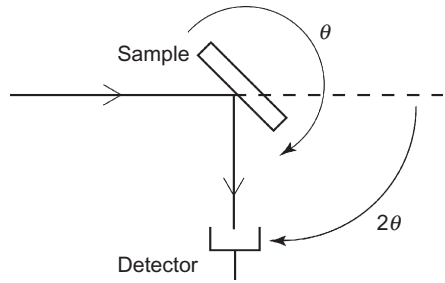

FIGURE 4.11 Schematic of the θ–2θ geometry angle-dispersive experiment commonly used in X-ray studies.

geometry, the sample remains stationary, and the source and the detector each rotate about the sample in such a way as to maintain a symmetric source-sample-detector arrangement. This geometry is less well suited to a synchrotron source! Diffractometers with these geometries are commercially available.

An alternative approach to collecting data for PDF studies is to use a Debye–Scherrer or Guinier camera. In the former case, the powder is placed in a capillary tube on the axis of a cylindrical container. Holes are cut in the container so that a collimated X-ray beam can enter and exit. An X-ray-sensitive film or image plate detector is then placed around the inside surface of the cylinder. They are described in much more detail in Klug and Alexander (1974). The Guinier camera is similar though the geometry is designed for optimizing monochromatic intensity, and resolution, from a divergent source (Klug and Alexander, 1974). A Guinier camera with a 100° angular range built-in image plate and reader is manufactured by Huber, for example.

4.3.3. X-ray Detection

Large area 2D detectors are required for RAPDF measurements. Initially, experiments were done using image plate technology, for example, the MAR345® detector. This can be thought of as electronic film since it works somewhat like X-ray film of years gone by, except that it can be exposed multiple times and erased and can be read out to give a digital signal without use of a densitometer. It combines a high dynamic range with a very low background and no dark current. The main disadvantage is the long readout time that is not well matched to the speed of data collection at modern PDF beamlines. The image plate contains a phosphor that absorbs the photons incident on it by creating metastable electronic defects (color centers). A readout laser is tuned to excite these defects and detect the subsequent radiation which is proportional to the number of defects that were created. The image is bleached after readout with a strong bleaching lamp and the IP can be reused. The material comes in flexible film form and can be cut, shaped, and bent (to some extent) and can be read out remotely (the image degrades slowly over time so it should be done a few minutes after exposure, and the exposure itself cannot be too long or the image is becoming lost even as it is being exposed) using image readers. The material is also somewhat light sensitive requiring careful handling. Infinitely more convenient are detectors with a built-in laser readout and bleaching setup such as the MAR345 and the Huber Guinier camera.

Large area 2D detectors with faster readout are available based on CCD and medical imaging technologies. CCD stands for charge coupled device and is a small electronic chip that is divided into pixels that can independently accumulate charge when they are excited by light. The charge in each pixel can be read out electronically by shunting the charge across a row of pixels.

The CCD chips cannot be scaled up to the large areas desired for these experiments (also direct exposure to intense X-rays tends to kill the chips) and so large area detectors are made by optically coupling a large area phosphor screen to the chip. There is an optic fiber that connects each pixel on the phosphor (which emits optical light when struck by an X-ray) to a pixel on the CCD chip. These detectors have reasonable dynamic range and fast readout but tend to be noisy and have significant dark current. The optical coupling also tends to introduce distortions into the image. The dark current is corrected by measuring dark (X-rays off) and light (X-rays on) exposures of the same length in pairs and subtracting the dark from the light. The optical distortions are corrected by a calibration where a known image (e.g., of a fine grid) is exposed on the detector and the image distortion corrected by moving pixel intensities such that the original undistorted image is recovered in the corrected image. This calibration table is then stored and applied to all subsequent images. This is not as hard as it sounds since the calibration is generally carried out by the manufacturer. The ESRF Frelon detector is an example of such a detector. The medical imaging detectors also have fast readout. The detection layer is amorphous silicon with a thin phosphor layer deposited on the surface and the readout is electronic making use of transistors that are fabricated on the amorphous silicon. A related technology is the Pilatus detector of the Swiss light source where the detection layer is single-crystal silicon, though it could be other materials such as GaAs, directly electrically connected with small metal balls (called bump bonding) to the electronics layer. Typically these detectors have around 10^6 pixels and readouts in the millisecond range, and can tolerate high data rates of around 10^6/s/pixel. The Pilatus detector is considered as a photon counting rather than an integrating detector. It was developed for protein crystallography applications but looks very promising for PDF work, especially if the efficiency at high X-ray energy can be optimized. The amorphous silicon detectors do have much higher detection efficiencies than the MAR345 at high energies and the combination of intense beams, good efficiency, and fast readout means that datasets can be collected from strongly scattering samples as quickly as a few tens of hertz frequency (i.e., $\sim$30 frames/s) (Chupas *et al.*, 2007). An amorphous silicon detector deployed at beamline 11IDB at the APS is shown in Fig. 4.12.

It should be noted that the efficiency of the 2D detectors is not spatially homogeneous, even though ideally it should be. This does not pose a problem if one is interested in getting $S(Q)$, but this becomes a serious issue when one tries to obtain the anisotropic PDF as described in Section 3.4.2. Even an isotropic sample would look anisotropic because of the anisotropy of the detector itself. The simplest solution to this problem is to obtain two datasets, with the detector, or preferably the sample, rotated by 90° and obtain the average.

Detectors for point counting were described in some detail in the first edition of this book, but we describe them only briefly here. The most commonly

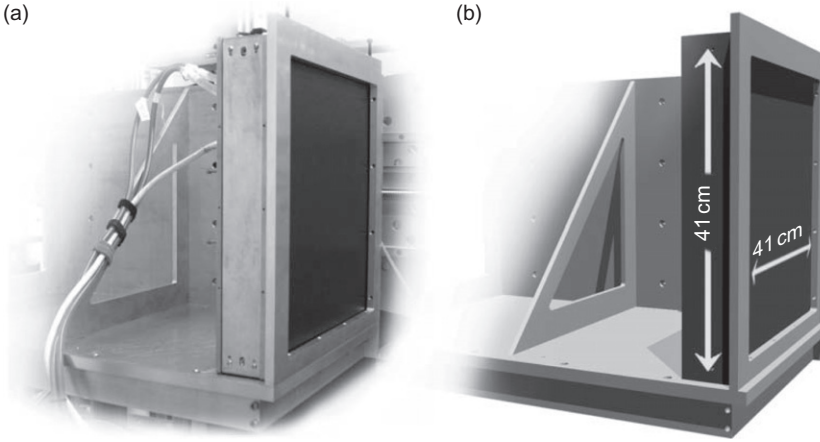

FIGURE 4.12 (a) Photograph and (b) CAD rendering of the large area amorphous silicon detector at beamline 11IDB at the Advanced Photon Source reproduced with permission (Chupas *et al.*, 2007).

used detector is a scintillation detector. This detector has poor energy resolution and cannot be used to discriminate inelastic scattering such as Compton scattering. A point detector that can discriminate Compton over most of the Q-range is a single-element or multi-element solid state detector (SSD). The main component of an SSD is a highly pure intrinsic semiconductor (Si or Ge) single crystal. Ge crystals are preferred for higher energy X-rays because of higher detection efficiency due to the more absorbing, higher atomic number, of Ge. An impinging photon creates an electron–hole pair that is swept out of the crystal by a large bias voltage and converted into a digital signal using pulse shaping electronics to measure the size of the charge (and therefore the photon energy) followed by an analog to digital converter. Currently, efforts are under way to extend this kind of detection technology to 1D and 2D detectors, sometimes called strip detectors. In this case, the electronics are usually in thin film form rather than a bulk single crystal, making detection efficiency of high-energy photons a major challenge.

A linear detector (PSD) is also useful in increasing the total count rate by parallel detection. Various forms of metal wire gas detectors (proportional counters) and semiconductor Si-diode array detectors are already available. Both have a relatively low-energy resolution (20–30%) and high background noise. Also, the normalization of the sensitivity of the wire detector is a nontrivial problem for quantitative measurements. The detection efficiency of a Si-diode detector drops quickly at high energies, and above 20 keV X-ray energies, they are practically transparent. Thus, they are rather unsuited for the high-Q measurements discussed here.

4.3.4. Beam Monitor

Monitoring of the incident beam intensity is important when a diffraction pattern is measured point by point because the diffraction intensities measured at each point will be proportional to this intensity which may be varying. This is not an issue when the full pattern is collected in parallel, such as in a RAPDF experiment. It may still be desirable to monitor the incident beam intensity if careful normalization between subsequent datasets is required, though this is rarely done as variations in incident beam intensity are corrected automatically during the normalization step of the processing anyway.

The most common method to monitor the beam is to place ion chamber detectors in the direct beam path. Ion chambers can count reliably at rates $\sim 10^6$/s with little dead time. The monitor must be stable. Ion chambers are stable if the gas flow through them is slow and constant. If the pressure in the ion chamber fluctuates too much, this can affect stability. The type of gas in the detector can be adjusted to increase efficiency depending on the incident energy, from nitrogen to argon to xenon. More details and alternative methods for X-ray beam monitoring can be found in the first edition of this book.

4.3.5. Measurement Geometry and Sample Issues

The RAPDF measurement geometry has been described in detail above. We briefly discuss aspects of some of the other powder diffractometer geometries. Geometries for laboratory sources are discussed in more detail in Klug and Alexander (1974).

Roughly speaking, any powder diffraction measurement carried out to sufficiently high Q can be used for a PDF measurement. One example is the high-resolution powder diffractometer, ID31 at ESRF which has a bank of multiple analyzer crystals (Fitch, 2004). It is mostly used for high-resolution powder diffraction for crystallographic analyses but can also be used to good effect for PDF studies because the beamline can be operated with quite short-wavelength X-rays. No special setup is required, though care should be taken to count for a long time in the high-angle region. The high resolution results in PDFs extending very far in r-space, hundreds of nanometers. The sample geometry in this powder diffractometer is cylindrical (the powders are in capillary tubes). At a synchrotron where the illumination is highly parallel, this is the preferred sample geometry. There is no advantage of having flat samples giving parafocusing of a divergent incident beam. This is also becoming the norm with laboratory X-ray machines that make use of highly efficient graded multilayer mirror optics that both monochromatize and steer the beam. We refer the interested reader to the first edition of this book for a more in-depth discussion of data collection geometries for divergent sources.

As with any powder samples, the particle size should be small (<40 μm) and uniform. This may be accomplished by careful grinding in a mortar and pestle and sieving the sample through a 400-mesh sieve. It is less relevant for nanoparticulate samples that do not have large coherently scattering grains. It is particularly important to avoid texture, preferential powder orientation, in the sample. This is generally easier when the particle size is smaller but can still be a problem if the powder grains have a particularly oblate or prolate morphology. Oblate samples are generally not a problem in capillaries, but needle-like samples can become significantly orientationally ordered in a capillary if the sample size is too big. Gentle grinding often takes care of the problem, but they could also be measured in the pill-shaped sample geometry described above to mitigate this problem.

Powders in pill form are often supported with thin kapton tape over the surface (Fig. 4.13). This is particularly important if the sample is to be cooled in a vacuum. Samples to be cooled may also be in kapton capillaries. Uncovered powders rarely survive the pump down as air trapped between the grains forces its way out. Differential thermal contraction between the sample holder and the powder itself can also loosen a tightly packed powder. A small amount of grease, or DUCO cement mixed with acetone, can also be mixed with a loose powder to stabilize it if the sample does not have to be recovered in its pristine state after the experiment. The scattering from the stabilizing agent is relatively weak. Traditional techniques of supporting a thin film of powder on a glass slide, widely used, for example, in sample characterization and *d*-spacing measurements, are unlikely to result in thick or uniform enough samples for the short-wavelength X-rays needed for PDF measurements.

FIGURE 4.13 Photograph of a flat-plate transmission sample supported between kapton foils.

4.3.6. Energy-Dispersive X-ray Diffraction Measurements

We briefly describe here some aspects of energy-dispersive X-ray diffraction measurements. The data collection and data analysis can be challenging but have been shown to be feasible (Egami, 1978) and, in cases where the take-off angle must be fixed, to be necessary. In the past, the use of this method was also valued because of the high intensity obtained from the white beam, making it attractive in cases where intensity was severely limited, for example, looking at amorphous materials in diamond anvil cells. However, the incredibly intense and small monochromatic beams at third- and fourth-generation synchrotron sources tend to make this argument less convincing now and even diffraction from diamond anvil cells is done with high-energy monochromatic beams in a RAPDF geometry.

In the case of X-ray scattering, the spectroscopy is most conveniently and quickly done by using an energy-sensitive SSD, such as a Li-drifted Si detector or an intrinsic Ge detector. These detectors have an energy resolution of about 1% that limits the Q-resolution. The spectrum from a diffracted white (non-monochromatic) beam includes not only the diffracted peaks but also other peaks such as the fluorescent peaks, escape peaks, and two-photon peaks, in addition to the inelastic Compton modified scattering intensity. The analysis of the spectrum has been described by Egami (1978).

4.4. THE ELECTRON PDF EXPERIMENT

Application of electron PDF methods to nanostructure determination is a relatively new development and practices and methods are likely to develop with time. However, we briefly describe here some aspects of the measurements that are pertinent for obtaining quantitative PDFs from nanosystems.

Apart from the strong scattering that leads to dynamical scattering effects that distort the kinematical diffraction pattern needed for PDF work, electrons lend themselves naturally to a PDF analysis. The wavelength of the electrons is short, typically a few hundredths of an angstrom for typical accelerating voltages, meaning that diffraction data to rather high values of Q appear in the forward scattering direction and can be detected on a typical electron microscope CCD camera. Because of the strong scattering, a reasonable signal can be obtained from a small volume of sample. This is both a blessing and a curse for PDF work. On the one hand, it means that very little material is needed to get a signal. On the other hand, it is harder to get a good powder average from the sample that is required for accurate PDF work. And, of course, the biggest challenge is ensuring sufficiently kinematical scattering. Because of the strong scattering, the probability of multiple scattering is high, and incoherent multiple scattering increases the background whereas the coherent multiple scattering process has to be described by the dynamical scattering theory. Nonetheless, the ubiquity of electron microscopes in

materials synthesis and characterization labs around the world, coupled with the very rapid data collection time for respectably high Q_{max} values (a few seconds compared to many hours to days for laboratory-based X-ray sources currently), is expected to make this approach for obtaining PDFs highly popular. There are many advantages of using intense synchrotron X-ray and neutron beams such that state-of-the-art experiments will continue to be carried out at these beamlines. However, the attraction of obtaining PDFs from nanomaterials rapidly and in your own laboratory, coupled with the fact that you can obtain low- and high-resolution images from precisely the same region of the sample that is probed by ePDF, is expected to make this approach very popular in the coming years.

There is a rich history of studying clusters in the gas phase and amorphous films using electron PDF methods, as discussed briefly in Section 3.1.4. For the case of gas phase electron diffraction, rather specialized modifications to the TEM are required, both for sample handling and for data collection. This is sufficiently far from the current topic that we do not go into this in detail. However, the study of amorphous thin films using electrons is much closer to the topic of this book. This work dates back to the pioneering work of Moss and Graczyk (1969) on amorphous silicon. The work used a custom designed and fabricated scanning diffraction attachment to a 100 keV TEM with energy filtering (Graczyk and Moss, 1969). It had high angular resolution and the energy filtering resulted in higher resolution as well as lower backgrounds. Detection was of charge in a Faraday cup or a p–n junction energy detector and the pattern was therefore obtained by changing the incident angle of the beam and scanning this, collecting data one point at a time. Following this, a number of authors took similar data on amorphous thin films using energy filtering and various electron detection methods (Chaudhari *et al.*, 1972; Rudee and Howie, 1972). Gandais *et al.* (1973) obtained diffraction patterns from amorphous Ge films without energy filtering by using an arduous method involving recrystallizing the film under electron irradiation and assuming the background scattering from the recrystallized film was the same as from the amorphous material that preceded it. The diffraction data were collected as an image on Kodak film under different magnifications to emphasize different Q-ranges. Because film has a rather narrow linear dynamic range, the flux on the sample had to be carefully controlled to prevent saturation. The film, after processing, was read with a microdensitometer. A system optimized for electron diffraction from amorphous materials (Cockayne and McKenzie, 1988) involved projecting the image of a selected area diffraction pattern onto the entrance aperture of a Gatan energy filter which is adjusted to select electrons of a particular energy (e.g., the elastic scattering). The pattern is then automatically stepped across the aperture to obtain the diffraction pattern. The scanning was accomplished with the use of deflection coils in the TEM column close to the back focal plane after the sample, inserted specifically for that task. An alternative arrangement used was to tilt the incident

beam, though this is not preferred as it changes the region of the sample illuminated, and therefore the volume of sample probed, on a point-by-point basis, introducing difficult-to-correct Q-dependent multiplicative errors. This approach was successfully used to verify the structure of the fullerene C_{70} (Mckenzie *et al*., 1992) (incidentally, the structure of C_{60} was also verified by electron diffraction, but in this case, in the gas phase; Hedberg *et al*., 1991), though the most accurate structures were obtained from neutron powder diffraction (David *et al*., 1991, 1993). This approach was also recently extended to deconvolute for the use of convergent beams, allowing very small spot sizes to be used and nanoscale sample volumes to be probed in amorphous materials without loss in angular resolution (McBride *et al*., 1999; Cai *et al*., 2002; McBride *et al*., 2003a,b; Oskaya *et al*., 2004; Petersen *et al*., 2005; McCulloch *et al*., 1999). In the more recent studies (McBride *et al*., 2003a,b; Oskaya *et al*., 2004; Petersen *et al*., 2005; McCulloch *et al*., 1999), a field emission gun microscope operating at 300 keV was used in nanodiffraction mode with energy filtering by a Gatan filter and detection using a CCD camera. This configuration combines excellent electron fluxes with a setup that is well matched to the needs of collecting data for PDF style work. This kind of electron microscope setup is still not ubiquitous but is becoming more common in laboratories around the world, which motivated the recent extension of these radial distribution function studies of amorphous materials to the world of nanomaterials dealt with in this book (Abeykoon *et al*., 2012).

Most of the work to date has been directed to the study of amorphous materials. However, the study of Abeykoon *et al*. (2012), briefly summarized in Section 5.3.9, addressed the extent to which nanocrystalline materials could be studied and how quantitatively reliable the resulting PDFs were for extracting accurate structural parameters through fitting using PDFgui and similar modeling programs discussed in Chapter 6. Furthermore, the possibility of obtaining accurate PDFs using modern transmission electron microscopes but without energy filtering was considered. This is facilitated by the development of accurate *ad hoc* data correction methods (Billinge and Farrow, 2012; Juhas *et al*., 2012) described in Section 5.2.1. The results look very promising, possibly opening up this approach to a much broader audience of nanomaterials scientists in the future. In some respects, the goal was to try and do the easiest and most broadly applicable experiment possible and see how high quality the resulting PDFs were using modern data reduction methods. With this in mind, a rather standard microscope was used and no energy filtering, although it is acknowledged that if energy filtering is available it should result in lower background and therefore better PDFs. The experimental ePDF from gold nanoparticles distributed on a holey carbon grid is shown in Fig. 4.14 with an excellent fit of fcc gold obtained using PDFgui plotted on top. This PDF was obtained with a rather standard Hitachi H8100 200 keV transmission electron microscope equipped with a Gatan Orius SC600 CCD Camera

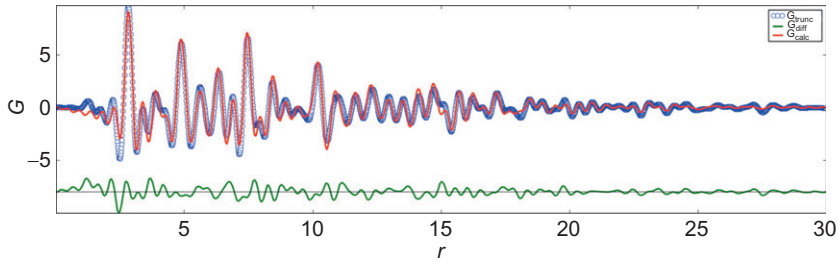

FIGURE 4.14 Open circles are the PDF of gold nanoparticles obtained using electron diffraction. The solid line is a calculated PDF from a structural model for the nanoparticles. The difference curve is shown offset below.

(24 mm × 24 mm active area). Typical exposure time per frame was around 0.3 s. It seems that rather high-quality PDFs can be obtained with rather unspecialized equipment using the *ad hoc* data correction protocols discussed in Chapter 5.

Below, we discuss some special considerations when collecting the data.

Sample preparation: Samples must be prepared somewhat carefully to avoid the effects of multiple scattering by having samples that are too thick. Luckily, the nanostructured samples for which a PDF study is of the greatest interest, when the particle size is below 10 nm, are the easiest to prepare by distributing the particles on a holey carbon grid. This can be straightforwardly accomplished by suspending the nanoparticles in a liquid that can be dripped onto the grid and allowed to evaporate. Nanostructured and polycrystalline thin films are another interesting application for the method. These must be electron transparent and just a few, to a few tens of, nanometers thick. It is important to avoid sample texture (i.e., preferred orientation of crystallites). Normally, this is not a problem for very small nanocrystals, though slightly larger crystallites may be faceted which tends to introduce a texture.

Powder average: Obtaining a reasonable powder average is essential in a PDF measurement. This was not a problem when studying amorphous materials but becomes a concern for ePDF measurements on nanocrystalline materials. A number of approaches may be taken to improve the powder statistics. If beam damage is not a concern, and if there are not features in the sample that cannot be avoided such as the copper support grid, then it is desirable to use as large a selected area as possible for obtaining the diffraction pattern. The area depends on the beam size, or as we describe below, is selected using an aperture. The powder statistics may be improved by tilting the sample and taking new images from the same area and also by moving the beam in between exposures to capture a different region of the sample. It is straightforward to assess the powder average by a visual inspection of the diffraction pattern to see if it is spotty or if the rings are continuous. This inspection

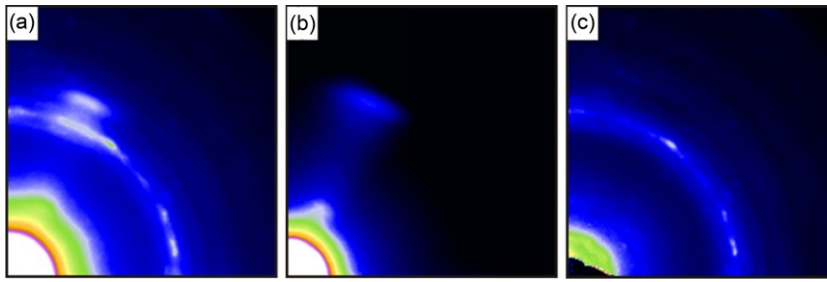

FIGURE 4.15 Electron diffraction patterns collected on a nanocrystalline sample. (a) Sample plus support. (b) Diffraction pattern of the support. (c) Diffraction pattern after subtracting the support. In this case, the largest background comes not from the support but from a ghost image of the electron source. However, this is reproducible and can be readily subtracted to obtain a spherically symmetric (except for imperfect powder averaging) diffraction pattern.

should be done after the multiple exposures are averaged as it is the powder average in the final summed data rather than the powder average in a single exposure that is critical. The azimuthal integration of the signal during the processing provides an additional averaging over the powder statistics and so a slightly spotty ring can be tolerated, as seen in Fig. 4.15c.

Camera length: Obtaining a reasonably high $Q_{\max}$ (preferably, in the region of 20 Å^{-1} or higher) results in much more useful PDFs. To this end, selecting the shortest possible camera length is desirable. As we discuss in the data correction section in Chapter 5, the camera length depends on the microscope lens settings. A calibration to measure the camera length is carried out by measuring a calibration sample of known lattice parameter. It is important to carry out the calibration measurements under precisely the same conditions, including all the lens currents, as the experiment on the sample itself. If nonstandard settings are used, this may be difficult, but an approach is to use calibration curves that correct for camera length for different lens current settings (Kolb *et al.*, 2011). If this calibration curve has been obtained by systematically varying lens settings on a known calibration sample, then when the diffraction pattern is obtained from the sample, it is simply required to record the current values and the camera length can be read off from the calibration curve. Alternatively, as mentioned in Chapter 5, an internal calibrant may be included when measuring the sample, or if accurate lattice parameters are not desired in the study, the sample itself may be used as a self-calibrant.

Data collection modes: The easiest mode to collect data in is selected area electron diffraction (SAED) mode. In this mode, the beam illuminates the sample but only a specific region of the sample is used to create the diffraction pattern by inserting an aperture. Intuitively, this would be done with a circular aperture inserted into the beam above the sample, but often in

practice, the aperture is placed after the sample. The two geometries are equivalent from the perspective of selecting an area of the sample from which to obtain a diffraction pattern, and this area can be moved around from place to place on the sample. The two are not equivalent from the point of view of sample damage, since in the latter case, a much larger area of the sample is being exposed to the incident beam than is actually being used to obtain the diffraction pattern. Where sample damage is an issue, in SAED mode, it is desirable to match the actual physical incident beam size to the size of the SAED aperture (in which case the aperture is not strictly needed) so that no unnecessary illumination of the sample takes place. The highest Q-resolution will be obtained when the incident beam is in a parallel beam illumination condition, and converging the beam to a smaller spot size lowers the Q-resolution. As we discuss elsewhere in this book, Q-space resolution is not usually a limiting factor for the quality of resulting PDFs, and other factors also play a role in the Q-space resolution such as pixel resolution on the detector, and so this is often a good trade-off. For good powder and counting statistics, beam sizes of the order of a micron are desirable. This approach of limiting the beam size to reduce beam damage may be taken to much more of an extreme by converging the beam to nanometer sizes and carrying out data collection in "nanodiffraction" mode. This has been done to enormously good effect when studying spatial variations in samples with an amorphous signal where powder averaging is not an issue (McBride *et al*., 1999; McBride *et al*., 2003a,b; Oskaya *et al*., 2004; Petersen *et al*., 2005; McCulloch *et al*., 1999). In these studies, the Q-resolution was also improved by deconvoluting the known beam convergence. The use of a nanodiffraction data collection is also a possibility when studying nanocrystalline materials, though it exacerbates the problem of determining the diffraction pattern with sufficient powder statistics. This was addressed in a study by Gorelik *et al*. (2012) where a nanodiffraction mode was used but multiple diffraction images taken by rastering the nanosized incident beam across a grid of positions on the sample so that a square 1 μm on the side was probed by systematically shifting the beam by the beam diameter in a 2D raster. The only advantage of this in the current context is to avoid unnecessary beam damage.

Detector: It is important to obtain quantitatively accurate diffraction patterns, which means ensuring that all intensities lie in the dynamic range of the detector where its response is linear. This means maintaining short exposure times. This is especially true when no energy filtering is done as the inelastic background in the low-Q region can be quite high. In order to determine low-intensity features with sufficient statistics, it is then necessary to make multiple exposures and to average the intensities. Electronic 2D detectors such as CCDs are adequate for measuring the electron diffraction, though image plates may be preferred if they are available as they have lower dark current and higher dynamic range. However, because of the small physical size of the diffraction pattern in the TEM the image plate must be read out

with a rather high spatial resolution or the angular resolution of the resulting 1D diffraction pattern is limited by the IP readout. Two approaches may be taken to avoid saturation (and damage!) of the detector. Either a beam stop may be used or the center of the beam may be located off the edge (or better, off the corner) of the CCD detector. An additional advantage of this latter geometry is that a greater Q-range is accessible for the same wavelength and camera length. Also, beam stops can become charged if not well grounded which deflects the scattered beam and introduces distortions into the diffraction pattern close to the beam stop. This is quite readily overcome in the data corrections (see Chapter 5) but is better to be avoided.

Sample support measurement: It is desirable to measure the background signal coming from any sample support (e.g., an holey carbon grid) where there is one. This can be done by moving the beam around until a region is found that is free of nanoparticles and collecting a diffraction pattern from this region. There are additional sources of background in the signal, as shown in Fig. 4.15, where a ghost image of the electron sources is evident as a non-spherically symmetric intensity. This is well reproduced in both the signal and the background and can be quite well subtracted, as shown in Fig. 4.15c. Thus, when collecting data, it is desirable if possible to find a region where no sample exists for collecting a good background. This can be borne in mind when creating the sample in the first place, so that some region of the holey carbon film is left free of material.

Energy filtering: If an energy filter is available on the microscope it is preferable to utilize it for removing, as much as possible, inelastically scattered electrons from the diffraction pattern. Here, we do not refer to the coherent inelastic scattering due to phonons in the material but due to electronic processes such as plasmons and atomic electronic transitions. Thus, typically, an energy window of 5–10 eV may be set bracketing the energy of the elastically scattered electrons. This will significantly reduce backgrounds in the data. However, Abeykoon *et al.* (2012) have shown that using modern processing methods this is not essential.

Multiple scattering: When multiple scattering is incoherent, it is relatively easy to correct for it and still retain kinematical scattering as we discuss in Chapter 5. Where desired, more accurate assessments of the multiple scattering correction can also be made by collecting diffraction data as a function of energy, using an energy filtering process, as described by Petersen *et al.* (2005), or by making multiple measurements on samples of different controlled thicknesses (Anstis *et al.*, 1988). Multiple scattering may also be reduced by using a precession technique where the electron beam it tilted with respect to the sample and the azimuthal angle varied rapidly to process the beam around the average direction. Some degree of multiple scattering can actually be tolerated and still obtain useful semiquantitative PDFs (Abeykoon *et al.*, 2012). This needs to be studied more systematically in the future so that incorrect conclusions are not drawn from data due to aberrations from

multiple scattering. However, some less important structural parameters seem to be affected most by the multiple scattering meaning that the PDF is somewhat tolerant to modest multiple scattering in the signal. One of the interesting effects of the multiple scattering is to shift coherent scattering intensity to the high-Q region of the pattern (Abeykoon *et al.*, 2012), which may actually prove to be an advantage in some situations since this is where the signal is normally weak and dominated by noise. Somewhat ironically, the big problem with electron diffraction for PDF studies, multiple scattering, actually produces an aberration whose main effect is artificially to increase the real-space resolution of the measurement! That being said, when making the sample, it is important to strive to minimize multiple scattering effects by avoiding samples that are too thick and particle sizes that are too large. Happily, the samples that are of most interest for PDF with nanocrystalline domains < 10 nm are precisely the ones that scatter with tolerable amounts of multiple scattering. Ideally, the samples should be less than a monolayer thick.

Beam damage: Another drawback of the strong interaction of electrons with materials is the harsh conditions that the sample is exposed to in the experiment. In general, it has to sit in a vacuum and is bombarded by an energetic beam of electrons that can cause considerable damage. This is especially relevant for organic materials. Beam damage can be reduced by cooling the sample to cryogenic temperatures, lowering the accelerating energy of the beam, reducing the fluence of electrons in the beam, and reducing the time the sample is exposed to the electron beam. Beam damage can also be assessed by observing a feature in the diffraction pattern as a function of time under different illumination conditions. In this way, it is possible to find conditions of current and exposure when one can be reasonably confident that the resulting diffraction pattern is not subject to modification due to the beam. As discussed above in the section on data collection modes, if beam damage is an issue for the sample, then it is also better to use data collection modes such as nanodiffraction, or SAED but with the incident beam diameter matched to the SAED aperture diameter, to avoid unnecessary illumination of the sample with the electron beam.

APPENDIX A4.1. EXPERIMENTAL CONSIDERATIONS FOR POINT-BY-POINT DATA COLLECTION

Although the vast majority of X-ray PDF experiments use the RAPDF method or another dedicated setup such as the powder diffractometer at ID31 at ESRF, it is worth retaining the details of how to set up such an experiment for those times where it is needed, especially at lower energy sources where the RAPDF approach is not feasible.

Here, we assume that a powder diffraction measurement is being set up with the sample at the sample being most likely a capillary sample or a flat plate in transmission or in reflection, depending on the circumstances. The

incident beam is monochromated by a crystal in the incident beam. There are slits before and after the sample that define the incident beam and collimate the scattered beam.

A number of factors affect the slit openings of the exit slits before the sample and the receiving slits before the detector. The X-ray measurements are generally higher resolution than neutron measurements. In PDF measurements, it is therefore possible to compromise the resolution to obtain higher intensities by working with a relatively large beam height (defined by the exit slit opening) and receiving slit opening. Values of 1–2 mm are typical for in-house setups and 0.5–1 mm at synchrotron sources. In the latter case, larger beam sizes would be preferred but are limited by the natural beam height. In this case, slits are still used to physically define the beam and to try and select a more uniform beam profile and polarization from the center of the beam. For ease of data analysis, it is often the case that data are collected in steps of constant ΔQ, though steps of constant $\Delta 2\theta$ can also be used. The step size depends on the resolution of the measurement. It is important to collect enough points that the step size is always smaller than the instrument resolution so all of Q-space is probed. The resolution varies with Q. It is set by a variety of factors such as sample size and beam divergence, but in a synchrotron experiment, the beam height is an important factor. The uncertainty in the scattering angle $\Delta 2\theta \sim h/L_2$ where h is the height of the beam and L_2 is the length of the secondary flight path from the sample to the receiving slit. Since $Q = 4\pi \sin\theta/\lambda$, the resolution in Q due to the finite beam size is given by

$$\Delta Q = \left(\frac{2\pi}{\lambda}\right)\cos\left(\frac{2\theta}{2}\right)\Delta 2\theta = \left(\frac{2\pi h}{\lambda L_2}\right)\cos\theta. \tag{A4.1}$$

This equation reflects the fact that the resolution gets better at high angle, a widely known result.[3] In principle, to maintain a constant resolution, the receiving slit width should be increased with angle. This has the added benefit of increasing statistics in the important high-Q region. However, this is seldom done in practice because of the difficulty of normalizing data correctly when the receiving slit width is changed in the middle of a measurement, as well as the obvious additional complexity of the measurement.

One thing to make sure of is that none of reciprocal space is missed in the measurement. Obviously this means that the angular step size, $\delta 2\theta$, must be less than $\Delta 2\theta$ or h/L_2. If the measurement is carried out in steps of constant 2θ, this is easily accomplished. However, if the measurement is carried out in steps of constant δQ, then some care must be exercised because the step size, $\delta 2\theta$, will change with angle. From Eq. (A4.1), we get

3. This is also true in tof neutron measurements where the backscattering detectors have much higher resolution than the low-angle detectors.

$$\delta Q < \Delta Q_{\min} = \left(\frac{2\pi h}{\lambda L_2}\right)\cos\,\theta_{\max}. \tag{A4.2}$$

Higher resolution measurements with smaller receiving slits and smaller step sizes are rarely warranted in the case of X-rays since the Fourier transform controls the frequency at which the data are sampled. Higher Q-space resolution results in PDFs extending to higher r which is almost never the limiting factor in a measurement.

Good collimation after the sample is desirable to minimize background from air scattering and sample environments such as heat shields and windows in vacuum shrouds. This is often accomplished with a set of slits positioned fairly close to the sample (sometimes known as scattering slits). However, care must be taken to ensure that the sample is well aligned in the center of the diffractometer circle so that at no time in the measurement is the sample shadowed by the scattering slits. This is particularly relevant in a PDF measurement where data are collected over such a wide range of scattering angles (typically $0.5^\circ < 2\theta < 135^\circ$). This shadowing is disastrous since it introduces an unknown Q-dependent modulation in the measured intensity which makes the data virtually impossible to correct. The primary role of this collimation is to eliminate parasitic scattering rather than to increase resolution by limiting divergence so there is no particular advantage in using Soller slits.

In a high-energy measurement, there can be a great deal of penetrating stray scattering in the experiment hutch during the measurement. It is important to minimize the effect of this on the measurement itself. This is done by limiting the amount of stray scattering by shielding the beam and covering beamline components which cause scattered radiation (e.g., slits) with lead. Finally, the detectors must be well shielded with lead to avoid X-rays entering the detector from another direction than the sample position. The usual construction of commercial semiconductor detectors is to mount the crystal in an aluminum housing that is woefully inadequate for keeping at bay 60 keV X-rays.

APPENDIX A4.2. INSTRUMENT ALIGNMENT

By way of example for those unfamiliar with instrument alignment, we give below a typical set of steps taken to align the diffractometer before beginning measurements. We are assuming a flat-plate transmission measurement at a synchrotron source. However, many of the principles are common to other geometries and sources.

Ensure the sample is at the mechanical center of the diffractometer. This is usually done by centering a pin at the sample position. The pin is viewed through a cross-hair telescope while being rotated. The sample mount is then translated in two directions perpendicular to the beam direction until no

parallax is observed. If a low-temperature stage is being used, this must be done with the cold stage in place.

Select beam energy and optimize the intensity at this energy. Monochromators at modern synchrotron sources tend to be two-crystal double bounce geometry. A number of alignments are necessary including vertical and horizontal offset, as well as lateral and longitudinal rotations. These all affect beam position, uniformity, and intensity. Upstream slits are generally set at this point, for example, the slits before and after the monochromator. These slits do not define the beam and so should not be set too tightly. Make sure the hottest part of the beam is not being cut and that the beam intensity profile is approximately symmetric. Other upstream beam conditioning optics should also be set and aligned such as monochromator focusing and harmonic rejection mirrors, although these are rarely used at the energies of interest for PDF measurements. These alignments are often carried out by beamline staff.

Center the beam on the pin at the center of the diffractometer. At a synchrotron, the diffractometer table has to be translated up and down to do this. The pin from step 1 is used and checked to see that it shadows the beam.

Set the exit slits (last slits before the sample) to the desired opening and center them on the beam and the pin. These slits should be independent of the diffractometer. These slits define the beam height and the beam position. After alignment, they should not be moved (or bumped!).

If it is not known, measure the detector dead times, τ. This is best done with a series of calibrated foils of known material and (uniform) thickness. These are systematically placed in front of the detector and the count rate (normalized by the monitor) recorded for each successive foil added. The data are fitted to the equation for detector dead time $I = I_0/(1 + I_{\text{tot}}\,\tau)$. Detector dead time can also be estimated dynamically during the experiment with the use of an electronic pulsar, or using the MCA "live time/real-time" ratio, as we describe later.

Set the receiving slits. These slits sit right in front of the detector. They should be set to the desired opening (see the discussion in Appendix A4.1) and centered on the detector, as close as possible to the axis of the 2θ diffractometer arm.

Find the $2\theta = 0$ position. Avoid destroying the detector by putting direct beam into it when doing this alignment! The object is to find the nominal angle when the direct beam is in the center of the detector receiving slit. This is done by measuring the direct beam profile by scanning the receiving slit, with an ion chamber detector behind it, or the SSD with a lot of attenuation in the beam, through the direct beam. Another useful setup is a silicon photodiode mounted on a strongly absorbing plate, such as hevimet, that can tolerate the intense direct beam and can be placed in front of the detector. The beam profile should be symmetric (if the beam is well aligned) and the center of the peak is the $2\theta = 0$ position. It is worthwhile after finding the $2\theta = 0$ position and setting the diffractometer software to zero 2θ at this position,

to record the physical angles from the diffractometer circles and motors. In this way, the integrity of the 2θ-zero can be easily checked at various times during or after the measurement without having to remeasure it. This is sometimes useful to reassure oneself that none of the circle motors has slipped or missed steps at any time.

Remove the aligning pin and install the sample on the diffractometer. The sample position must be reliable and reproducibly close to the position of the pin. This is usually done by carefully machining the sample mount to ensure the center of diffraction of the sample is at the same position as the pin. In a transmission sample, this will be the center of the sample. In a reflection sample, it will depend on the thickness and penetrability of the sample (and on the scattering angle) but is likely to be somewhere between the center of the sample and the front face. This complication means that it is unwise to make a reflection sample more than a few millimeters thick at most, even if this means that the sample has a finite transparency.

Measure μt of the sample. The easiest way is with the sample perpendicular to the beam measure the direct beam intensity (normalized by the monitor) with and without the sample in place. Another approach is to rotate the flat-plate sample through $\pm 60^\circ$ while recording the intensity (remember, do not put direct beam into a sensitive detector). The resulting intensity will have the form $\ln(I/I_0) = -\mu t/\cos\theta$; thus plotting $\ln(I/I_0)$ versus $\sec\theta$ will give you a straight line of slope $-\mu t$.

Set the scatter slits. These are the slits that sit immediately after the sample. Find a strong Bragg peak from the sample. Bring in each blade of the slits separately until the intensity falls to zero. Record these positions which define the edges of the scattered beam. Set the scatter slits as close as you dare (but not too close) to the beam edges. Check the slits by studying a few Bragg peaks (or other features which give significant scattering) at widely separated scattering angles. If the sample is well aligned, the beam edges should be in the same positions independent of angle. Make sure the scatter slits are set so that the scattered beam is never cut by a slit. A wise experimenter errs on the safe side here.

Check the sample powder averaging. Measure a rocking curve at one or two Bragg peak positions. With the detector fixed at the 2θ of a Bragg peak, rock the sample (θ angle) back and forth through a few degrees recording the intensity. In general, the sample will have to be rocked to ensure good powder averaging. The intensity should be more or less constant (after normalizing for incident flux) and not fluctuate too greatly. This problem is especially acute at synchrotron sources where beam footprints can be very small.

Set the $\theta = 0$, position. In this position, the sample is parallel (perpendicular) to the beam in reflection (transmission). The $\theta = 0$ is set with the sample parallel to the beam and the detector at the $2\theta = 0$ position (again, care must be taken not to destroy the detector with the direct beam). In this position, the sample will shadow approximately half the beam. If the sample is rotated

in either direction by a small angle, the sample will completely shadow the beam. By scanning the θ angle through zero with the detector held at $2\theta = 0$, a symmetric minimum should be apparent in the intensity. This alignment is not crucial in a powder measurement and is often done by eye or with the help of a spirit level.

REFERENCES

Abeykoon, M., Malliakas, C.D., Juhas, P., Bozin, E.S., Kanatzidis, M.G. & Billinge, S.J.L. (2012) *Z. Kristallogr.*, **227**, 248.

Anstis, G.R., Liu, Z. & Lake, M. (1988) *Ultramicroscopy*, **26**, 65.

Bacon, G.E. (1975) *Neutron Diffraction.* Oxford: Clarendon Press.

Billinge, S.J.L. & Farrow, C.L. (2012) To be published.

Bowron, D.T., Soper, A.K., Jones, K., Ansell, S., Birch, S., Norris, J., Perrott, L., Riedel, D., Rhodes, N.J., Wakefield, S.R., Botti, A., Ricci, M.A., Grazzi, F. & Zoppi, M. (2010) *Rev. Sci. Instrum.*, **81**, 033905.

Bozin, E.S., Juhas, P., Zhou, W., Stone, M.B., Abernathy, D.L., Huq, A. & Billinge, S.J.L. (2009) *J. Appl. Crystallogr.*, **42**, 724.

Caglioti, G., et al. (1958) *Nucl. Instrum.*, **3**, 223228.

Cai, Y., Prinz, S., Zimmermann, A., Zern, A., Sigle, W., Rühle, M. & Aldinger, F. (2002) *Scr. Mater.*, **47**, 7.

Carpenter, J.M. (1977) *Nucl. Instrum. Methods*, **145**, 91.

Chaudhari, P., Graczyk, J.F. & Herd, S.R. (1972) *Phys. Status Solidi (h)*, **61**, 801.

Chirawatkul, P., Zeidler, A., Salmon, P.S., Takeda, S., Yukinobu, K., Usuki, T. & Fischer, H.E. (2011) *Phys. Rev. B*, **83**, 014203.

Chupas, P.J., Chapman, K.W. & Lee, P.L. (2007) *J. Appl. Crystallogr.*, **40**, 463.

Chupas, P.J., Qiu, X., Hanson, J.C., Lee, P.L., Grey, C.P. & Billinge, S.J.L. (2003) *J. Appl. Crystallogr.*, **36**, 1342.

Cockayne, D.J.H. & McKenzie, D.R. (1988) *Acta Cryst. A*, **44**, 870.

David, W.I.F., Ibberson, R.M. & Matsuo, T. (1993) *Proc. R. Soc. London Ser. A*, **442**, 129.

David, W.I.F., Ibberson, R.M., Matthewman, J.C., Prassides, K., Dennis, T.J.S., Hare, J.P., Kroto, H.W., Taylor, R. & Walton, D.R.M. (1991) *Nature*, **353**, 147.

Drewitt, J.W.E., Salmon, P.S., Barnes, A.C., Klotz, S., Fischer, H.E. & Crichton, W.A. (2010) *Phys. Rev. B*, **81**, 014202.

Egami, T. (1978) *J. Mater. Sci.*, **13**, 2587.

Farrow, C.L. & Billinge, S.J.L. (2009) *Acta Crystallogr. A*, **65**, 232.

Fischer, H.E., Cuello, G.J., Palleau, P., Feltin, D., Barnes, A.C., Badyal, Y.S. & Simonson, J.M. (2002) *Appl. Phys.*, **74**, s160.

Fischer, H.E., Howells, S. & Salmon, P.S. (2012) *Workshop on Analysis of Diffraction Data in Real Space (ILL, Grenoble, 12–14 Oct 2011).*

Fitch, A. (2004) *J. Res. NIST*, **109**, 133.

Gandais, M., Theyes, M.L., Fisson, S. & Boissona, J. (1973) *Phys. Status Solidi (b)*, **58**, 601.

Gorelik, T.E., Schmidt, M. & Billinge, S.J.L. (2012) Unpublished.

Graczyk, J.F. & Moss, S.C. (1969) *Sci. Instrum.*, **40**, m4.

Hannon, C. (2005) *Nucl. Instrum. Methods A*, **551**, 88.

Hedberg, K., Hedberg, L., Bethune, D.S., Brown, C.A., Dorn, H.C., Johnson, R.D. & Vries, D.E.M. (1991) *Science*, **254**, 410.

Hennet, L., Pozdnyakova, I., Bytchkov, A., Cristiglio, V., Palleau, P., Fischer, H.E., Cuello, G.J., Johnson, M., Melin, P., Zanghi, D., Brassamin, S., Brun, J.F., Price, D.L. & Saboungi, M.L. (2006) *Rev. Sci. Instrum.*, **77**, 053903.

Hewat, A.W. (1975) *Nucl. Instrum. Methods*, **127**, 361370.

Ishigaki, T., Hoshikawa, A., Yonemura, M., Morishima, T., Kamiyama, T., Oishi, R., Aizawa, K., Sakuma, T., Tomota, Y., Arai, M., Hayashi, M., Ebata, E., Takano, Y., Komatsuzaki, K., Asano, H., Takano, Y. & Kasao, T. (2009) *Nucl. Instrum. Methods A*, **600**, 189.

Juhas, P., Dykhne, T., Farrow, C.L. & Billinge, S.J.L. (2012). To be published.

Klug, H.P. & Alexander, L.E. (1974a) *X-ray Diffraction Procedures* (2nd Edition). New York: Wiley.

Kolb, U., Mugnaioli, E. & Gorelik, T.E. (2011) *Cryst. Res. Technol.*, **46**, 542.

McBride, W.E., Cockayne, D.J.H. & Goringe, C.M. (1999) *Ultramicroscopy*, **76**, 115.

McBride, W.E., Cockayne, D.J.H. & Ngyun-Manh, D. (2003a) *Ultramicroscopy*, **96**, 191.

McBride, W.E., Cockayne, D.J.H. & Tsuda, K. (2003b) *Ultramicroscopy*, **94**, 305.

McCulloch, D.G., McKenzie, D.R., Goringe, C.M., Cockayne, D.J.H., McBride, W.E. & Green, D.C. (1999) *Acta Crystallogr. A*, **55**, 178.

McKenzie, D.R., Davis, C.A., Cockayne, D.J.H., Muller, D.A. & Vassallo, A.M. (1992) *Nature*, **355**, 622.

Moss, S.C. & Graczyk, J.F. (1969) *Phys. Rev. Lett.*, **23**, 1167.

Neuefeind, J., Feygenson, M., Carruth, J., Hoffmann, R. & Chipley, K.K. (2012) *Nucl. Instrum. Methods B*, Submitted.

Oskaya, D., McBride, W.E. & Cockayne, D.J.H. (2004) *Interface Sci.*, **12**, 321.

Petersen, T.C., McBride, W.E., McCulloch, D.G., Snook, I.K. & Yarovsky, I. (2005) *Ultramicroscopy*, **103**, 275.

Proffen, T., Egami, T., Billinge, S.J.L., Cheetham, A.K., Louca, D. & Parise, J.B. (2002) *Appl. Phys. A*, **74**, s163.

Rudee, M.L. & Howie, A. (1972) *Philos. Mag.*, **25**, 1001.

Schull, C. (1995) *Rev. Mod. Phys.*, **67**, 753.

Westfall, C.W. (2007) Argonne National Laboratory, ANL/HIST 5.

Williams, W.G., Ibberson, R.M., Day, P. & Enderby, J.E. (1998) *Physica B*, **241–243**, 234.

Willmott, P. (2011a) *An Introduction to Synchrotron Radiation: Techniques and Applications*. West Sussex: Wiley & Sons.

Zeidler, A., Drewitt, J.W.E., Salmon, P.S., Barnes, A.C., Crichton, W.A., Klotz, S., Fischer, H.E., Benmore, C.J., Ramos, S. & Hannon, A.C. (2009) *J. Phys. Condens. Matter*, **21**, 474217.

4.5 SELECTED BIBLIOGRAPHY

Spallation neutrons and sources

Willis, B.T.M. & Carlile, C.J. (2009) *Experimental Neutron Scattering*. Oxford: Oxford University Press.

Windsor, C.G. (1981) *Pulsed Neutron Scattering*. London: Taylor & Francis.

Newport, R.J., Rainford, B.D., & Cywinski, R. (Eds.), (1988). *Neutron Scattering at a Pulsed Source*. Bristol: Hilger Somewhat out of date but useful background information. Lectures given at the Summer School on Neutron Scattering at a Pulsed Source held at the Rutherford Appleton Laboratory (ISIS) and in Mansfield College, Oxford, for the period 16–24 September 1986.

The ISIS Web site has a nice introduction to spallation and pulsed neutron scattering: http://www.isis.rl.ac.uk.

Synchrotron X-rays and sources:

Als-Nielsen, J. & McMorrow, D. (2011) *Elements of Modern X-ray Physics* (2nd Edition). West Sussex: Wiley & Sons.

Ciocci, F., Torre, A. & Dattoli, G. (2000) *Insertion Devices for Synchrotron Radiation and Free Electron Laser*. Singapore: World Scientific.

Duke, P.J. (2000) *Synchrotron Radiation: Production and Properties*. Oxford: Oxford University Press.

Mills, D. (2001) *Third Generation Hard X-ray Synchrotron Radiation Sources Properties, Optics, and Experimental Techniques*. New York: Wiley.

(2000) *Synchrotron Light to Explore Matter*. Berlin: Springer.

Willmott, P. (2011b) *An Introduction to Synchrotron Radiation: Techniques and Applications*. West Sussex: Wiley & Sons.

X-ray and neutron detection:

Brief introductions are available in many introductory books on X-ray and neutron scattering, for example, Klug and Alexander (1974) for X-rays and Bacon (1975) for neutrons. One of the best ways to learn about details of X-ray detection is to read the tutorial sections of the product catalogs of the main detector manufacturers such as Ortep and Canberra, or to consult their Web sites. Otherwise books tend to be rather specialized and/or out of date such as: Allen, W.D. (1960) *Neutron Detection, Philosophical library*, New York; or Combes, C (1999) *Scintillation Properties of ^{6}Li-based Materials for Thermal-neutron Detection*, Coronet Books.

Powder diffraction and diffractometry:

Jenkins, R. & Snyder, R.L. (1996) *Introduction to X-ray Powder Diffractometry*. New York: Wiley.

Klug, H.P. & Alexander, L.E. (1974b) *X-ray Diffraction Procedures* (2nd Edition). New York: Wiley.

Young, R.A. (1995) *The Rietveld Method*. Oxford: Oxford University Press.